MODELING OF CONDENSATION PROCESS INSIDE SMOOTH HORIZONTAL TUBES

A DISSERTATION

Submitted in partial fulfilment of the requirements for the award of the degree of

MASTER OF TECHNOLOGY

in

CHEMICAL ENGINEERING

(With Specialization in Computer Aided Process Plant Design)

By

ANIL KUMAR VERMA

DEPARTMENT OF CHEMICAL ENGINEERING
INDIAN INSTITUTE OF TECHNOLOGY ROORKEE
ROORKEE-247 667 (INDIA)

JUNE, 2005

CANDIDATE'S DECLARATION

I hereby declare that the work which is being presented in the dissertation entitled **"MODELING OF CONDENSATION PROCESS INSIDE SMOOTH HORIZONTAL TUBES"** in partial fulfilment of the requirements for the award of the degree of **MASTER OF TECHNOLOGY** in Chemical Engineering with specialization in Computer Aided Process Plant Design (CAPPD), submitted in the Department of Chemical Engineering, Indian Institute of Technology, Roorkee, is an authentic record of my own work carried out, under the guidance of **Dr. Bikash Mohanty**, Professor & Head, Department of Chemical Engineering and **Dr. Ravi Kumar**, Assistant Professor, Department of Mechanical and Industrial Engineering, Indian Institute of Technology Roorkee.

I have not submitted the matter embodied in this project report for the award of any other degree or diploma.

Date: 03/06/05

Place: Roorkee

(ANIL KUMAR VERMA)

CERTIFICATE

This is to certify that the above statement made by the candidate is correct to the best of our knowledge.

(Dr. RAVI KUMAR)

Assistant Professor
Department of Mech. and Ind. Engg.
Indian Institute of Technology
Roorkee-247667
INDIA

(Dr. BIKASH MOHANTY)

Professor & Head
Department of Chemical Engineering
Indian Institute of Technology
Roorkee – 247 667
INDIA

ACKNOWLEDGEMENTS

I avail this opportunity to express my deep sense of gratitude and sincere thanks to **Dr. Bikash Mohanty**, Professor & Head, Chemical Engineering Department, Indian Institute of Technology, Roorkee for invaluable guidance he rendered me during the course of my work. His constant encouragement and painstaking efforts have been the sole endeavours to bring this dissertation report in its present form.

I gratefully acknowledge my sincere thanks to **Dr. Ravi Kumar**, Assistant Professor, Department of Mechanical and Industrial engineering, Indian Institute of Technology, Roorkee, and my friends especially Prashant Kalkar, Saurabh Gupta and Dharmesh Chaudhari and members of my family for their inspirational impetus and moral support during the study of this work.

Date: 03/06/05

Place: Roorkee

(ANIL KUMAR VERMA)

ABSTRACT

The present dissertation work consists of the development of a mathematical model for the condensation of pure saturated vapours, inside a smooth horizontal tube. The condensation heat transfer coefficient based on the flow regime inside the tube has been obtained by computation. A new generalised heat transfer model for the condensation of pure vapours inside a horizontal smooth tube has been developed. In fact the model by Thome et al. (2003) has been modified based on simplified flow structures of the flow regimes.

The proposed model can predict local condensation heat transfer coefficient for the following flow regimes: annular flow, intermittent flow, stratified-wavy flow, fully stratified flow and mist flow. Further, the model has been developed for a large number of refrigerants like R-11, R-12, R-22, R-32, R-113, R-125, R-134a, R-404A, R-410A, and some of the hydrocarbons like propane, n-butane, iso-butane and propylene. The proposed model has been tested for mass velocity of 24 - 1022 kg $m^{-2}s^{-1}$, vapour quality 0.03 - 0.97, reduced pressure 0.02 - 0.8 and tube internal diameter 3.1 - 21.4 mm.

The flow pattern map of Taitel and Dukler (1976), modified by Hajal et al. (2003), has been used in present work to modify the model of Thome et al. (2003). The effect of various parameters i.e. mass velocity, vapour quality, void fraction, reduced pressure, the difference between the saturated temperature and the wall temperature etc. on the flow pattern map predictions and on the heat transfer coefficient are studied by using the present model. The proposed model is also tested on extreme values of vapour quality and different flow regime transition zones.

The flow pattern predictions are compared with the predictions of flow pattern from methods provided by Tandon et al. (1982), Dobson and Chato (1998), Soliman (1982) and Cavallini et al. (2002). The different void fraction models applied previously for flow pattern map prediction are studied and compared with present logarithmic mean void fraction model. Finally the condensation heat transfer coefficients obtained by present model for different refrigerants and hydrocarbons at different test conditions are

compared with the experimental results of different investigators. The predictions of present model are also compared with the predictions from other models for condensation inside smooth horizontal tubes viz. Cavallini et al. (2002), Shah (1979), Dobson and Chato (1998), and Aprea et al. (2003), which are widely accepted.

A comparison of the results from the proposed model shows better agreement with the experimental values in comparison to the predictions from the widely accepted Thome's model. The proposed model predicts the heat transfer coefficient within an error band of ± 17.5 percent for 80 percent of experimental data, whereas, the widely accepted Thome's model (2003) predicts the heat transfer coefficient within an error band of ± 20 percent.

CONTENTS

LIST OF FIGURES

NOMENCLATURE

Symbols	Description	Unit
A	cross sectional area	m^2
A_{Ld}	dimensionless cross sectional area for liquid phase	m^2
A_{Vd}	dimensionless cross sectional area for vapour phase	m^2
c	convective film constant	
Cp_L	specific heat of liquid	$J\ kg^{-1}K^{-1}$
d	tube internal diameter	m
f_i	interfacial roughness factor	
$F_1(q)$	empirical expression for effect on heat flux on dryout	
$F_2(q)$	-do-	
g	acceleration due to gravity	$m\ s^{-2}$
G	mass velocity	$kg\ m^{-2}s^{-1}$
G_{bubbly}	bubbly flow transition mass velocity	-do-
G_{mist}	mist flow transition mass velocity	-do-
G_{str}	stratified flow transition mass velocity	-do-
G_{wavy}	wavy flow transition mass velocity	-do-
h	heat transfer coeff., used in some references	$W\ m^{-2}K^{-1}$
h_{Ld}	dimensionless height of liquid film inside tube	
h_{LV}	latent heat of vaporisation	$J\ kg^{-1}$
k_L	thermal conductivity of liquid	$W\ m^{-1}K^{-1}$
p_{crit}	critical pressure	Pa
p_r	reduced pressure	
p_{sat}	saturation pressure	Pa

Symbols	Description	Unit
T_{sat}	saturation temperature	°C
T_w	wall temperature	°C
q	heat flux	W m^{-2}
u_L	mean liquid velocity in the film	m s^{-1}
u_V	mean vapour velocity	m s^{-1}
x	vapour quality	
x_{IA}	vapour quality at transition from intermittent to annular flow	
X_{tt}	Martinelli parameter with both phase turbulent	

DIMENSIONLESS NUMBERS

Fr_{SO}	Soliman's modified Froude number, Eqs. (2.9, 2.10)	
Ga	Galileo number, Eqs. (2.13)	
Ja_l	liquid Jakob number, Eqs. (2.14)	
Su	Suratman number, ($\rho_g D\sigma/\mu_g^2$)	
We_{SO}	Soliman's modified Weber number, Eqs. (2.11, 2.12)	

GREEK SYMBOLS

α_c	convective condensation heat transfer coefficient	W $m^{-2}K^{-1}$
α_f	Nusselt film condensing heat transfer coefficient on top perimeter of the tube	-do-
α_{tp}	local perimeter averaged condensing two-phase heat transfer coefficient	-do-
δ	liquid film thickness of annular ring	m
ε	void fraction of vapour	
μ_L	liquid dynamic viscosity	Ns m^{-2}

μ_V	vapour dynamic viscosity	-do-
θ	upper angle of the tube not wetted by the stratified liquid	rad
θ_{str}	stratified angle around upper perimeter of the tube	rad
ρ_G	vapour density	kg m^{-3}
ρ_L	liquid density	-do-
σ	surface tension	N m
τ_I	interfacial shear of vapour on liquid film	J m^{-3}
τ_w	wall shear stress	-do-
ξ	factor used in mist flow transition mass velocity	

SUBSCRIPTS

an, ann	annular flow
so	Soliman's modified no.
RA	Rouhani-Axelsson
tr	transition
str	stratified flow

Chapter 1

INTRODUCTION

Condensation is the process in which a vapour is converted to its liquid state. Because of the large total energy difference between the liquid and vapour state, a significant amount of heat is released during the condensation of vapours. In general, a vapour will condense to liquid state when it is cooled or comes in contact with the cold solid or liquid surface. The condensation process takes place in many thermal systems viz. power plants, refrigeration and air-conditioning systems and process industries.

There are numerous studies pertaining to condensation heat transfer in the literature [5-27]. These studies include physical efforts to model the physics of condensation process, experimental efforts to measure the heat transfer behaviour of certain fluids, and various combinations of the above. Most investigators have collected data for a limited number of fluids under a range of operating conditions that was suitable for the applications of their interest. Their own data were matched with existing correlations, and some investigators developed semi-empirical correlations with the help of their own data. Many correlations that are available come with no explicit range of parameters over which they can be expected to give accurate results. Although there are handbooks and design manuals supplying reasonable recommendations for a design engineer who is searching the technical literature, the overall literature provides seemingly diverse reports about which correlation is the 'best'.

There is an agreement in the literature that the mechanisms of heat transfer and pressure drop are intimately linked with the prevailing two-phase flow regime. This has led to many studies aimed at predicting what dimensionless parameters govern specific flow regime transitions and at what values of these dimensionless parameters certain transitions are expected to occur. Although debates still exist in the literature concerning differences in the flow regime predictions of various researchers, a basic understanding has been established of what the various flow regimes are and in most cases, what parameters are suitable for determining the transition from one flow regime to the next. Thus, the topics of heat transfer and flow regimes must be combined in the correlations that can be used in the design of condensers.

When two phases flow in a horizontal pipe, they can be distributed in the pipe in a number of different configurations. These configurations are called 'flow regimes', and the analysis of any two-phase flow problem begins by specifying the flow regimes. It has been found that, in order to reduce a two-phase flow problem to tractable proportions, it is necessary to combine some analytical methods with some experimental results.

One of the most striking characteristics of any two-phase flow is that, in general, the phases do not move with the same velocity. The gas phase velocity is normally higher than that of liquid phase. Because of this it has been found convenient to speak of a slip-velocity ratio. If this ratio is specified, then it is possible to determine the density of the mixture in pipe from the flow rates of each of the phases. At low pressure in particular, the vapour phase normally moves with many times the velocity of the liquid phase so that the static quality is much lower than the flowing quality.

When a cold surface at temperature, T_w, is exposed to a vapour at temperature, T_s, liquid condensate is formed on the surface. The exact nature of the condensation mechanism on a clean surface is not well established. One suggestion visualises the surface to embody small cavities containing liquid; this small liquid surface may be the site at which condensation begins. A finite amount of sub cooling would be required, the magnitude depending on the curvature of the small liquid surface.

If the liquid does not wet the surface macroscopically, the condensate forms liquid droplet. Then the surface is covered with alternate patches of dry and wet spots. If on the other hand the liquid wets the surface macroscopically, a continuous liquid layer covers the condensing surface. Since heat-transfer coefficients with film condensation are the smaller, commercial condensers are sized assuming film condensation will prevail.

Kattan et al. [1-3] proposed a new comprehensive flow boiling heat transfer model for evaporation inside plain horizontal tube, based on the newly developed diabatic flow pattern map. Their new approach resulted in very significant improvements in the accuracy and reliability of heat transfer predictions compared to previous methods. Based on the flow pattern identification of Kattan et al. [3] for boiling heat transfer model, Hajal et al. [4] have given the flow pattern prediction for condensation. They have used a new logarithmic mean void fraction method to identify and predict the different flow regimes

in condensation inside plain horizontal tube. Based on the method of flow regime prediction of Hajal et al. [4], Thome et al. [5] have presented a new heat transfer model for two-phase heat transfer coefficient. They have experimented over a large number of data points with different refrigerants and some hydrocarbons also.

1.1 OBJECTIVES OF THE THESIS

The objectives of the present study are:

(i) To arrive at a unified approach for modelling of flow patterns.

(ii) To obtain and apply a void fraction model, which is applicable for low pressure to high pressure ranges, and also up to critical pressure.

(iii) To modify the Thome et al. [5] model, this is most widely accepted in terms of its large range of parameters and applicability.

The aim of the present work is to calculate the heat transfer coefficients during condensation within plain horizontal tubes, and therefore a new version of the two-phase flow pattern map originally developed by Kattan et al. [3] for flow boiling and then modified by Hajal et al. [4] for condensation is utilized to predict the flow regimes inside horizontal tubes. Then a new modified condensation heat transfer model based on the model of Thome et al. [5] is presented. This model is predicting the heat transfer coefficient for two-phase flow in condensation inside plain horizontal tube with better accuracy, and more close to the experimental heat transfer coefficient database.

Chapter 2

LITERATURE REVIEW

The present study of two-phase flow heat transfer model is divided in two parts; first of all the development of flow pattern is studied and secondly the heat transfer models in the literature are discussed.

2.1 TWO-PHASE FLOW PATTERN MAP

Numerous flow pattern maps have been proposed over the years for predicting two-phase flow regime transitions in horizontal tubes. The map of Taitel and Dukler [6] and Baker [7] are perhaps those most quoted. Hashizume [8] and Mandhane et al. [9] have also given flow pattern map and void fraction prediction for two-phase flow. Specifically for condensation, flow pattern maps have been proposed by Breber et al. [10], by Tandon et al. [11], and recently by Cavallini et al. [12].

In addition numerous methods have been proposed to differentiate between stratified and non-stratified condensation, such as those by Ackers and Rosson [13], Sardesai et al. [14], Shah [15] and Dobson and Chato [16].

There are two factors controlling the flow viz. gravity and vapour shear. At low vapour velocities gravity dominates and the condensate forms primarily on the top portion of the tube and flows downward into a liquid pool which is driven out axially, partly by the vapour flow and partly by a gravitational head. In terms of void fraction, the flow regimes can be divided into the following two groups: (1) those that occur at high void fractions; and (2) those that occur only at low void fractions. The first category includes five flow regimes: stratified flow, stratified-wavy flow, intermittent flow, annular flow, and mist flow. The second category includes slug flow, plug flow, and bubbly flow. The five flow regimes in the first category are arranged such that each successive flow regime corresponds to an increase in the vapour velocity. Thus the first two are gravity dominated, the third is influenced about equally and the last two are vapour shear dominated. The three flow regimes in the second category are arranged such that the transition from one flow regime to next corresponds to an increase in the liquid inventory (i.e., decrease in void fraction). At very low vapour velocities the gravity controlled

stratified flow regime is observed. Because the vapour velocity is low, the liquid-vapour interface remains smooth.

As the vapour velocity is increased, the liquid-vapour interface becomes unstable, giving rise to surface waves and stratified-wavy flow. The condensation process on the top of the tube is similar to that in stratified flow. The condensation process on the portion of the tube near the interface between the liquid pool and the vapour is affected by the waves since it is alternately exposed to a thin condensate film flowing downward and the crest of a wave moving in the mean flow direction.

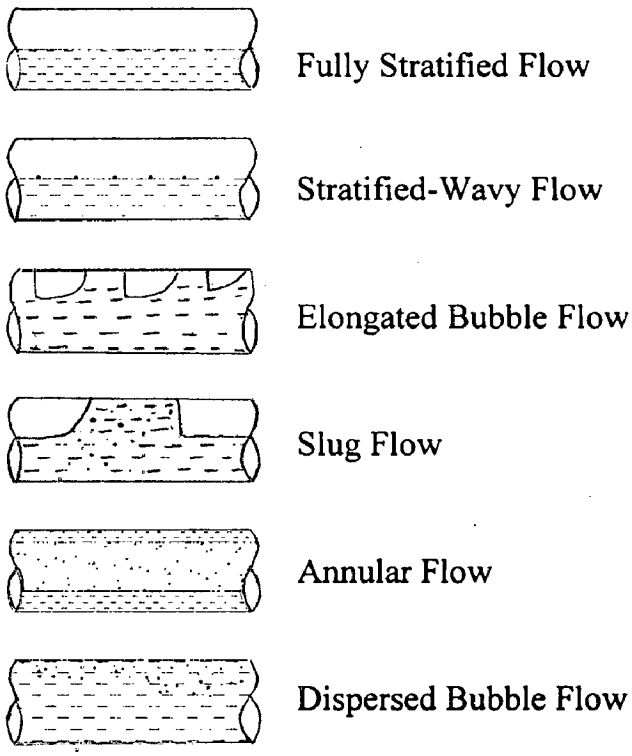

Fig. 2.1 Schematic diagram of flow patterns in horizontal tubes

As the vapour velocity is increased further, the stratified-wavy flow becomes unstable and can result in two different transitions. At high liquid fractions, the slug flow case that is described subsequently occurs. At lower liquid fractions, the waves begin to wash up and around the tube wall, leading to annular flow. Before the annular flow pattern is reached, however, a transitional flow pattern called intermittent flow is observed in which some liquid from the waves begin to wash up and around the circumference of the tube, but not enough to create a symmetric annular film. This liquid moves primarily in the

mean flow direction rather than downward, creating the primary difference from the stratified-wavy flow regime.

With still further increase in the vapour velocity, the liquid migration from the pool at the top of the tube continues until the film thickness becomes nearly uniform. The visual appearance of this type of flow is one of an annular film of liquid on the wall and high-speed vapour cores in the centre, hence the name annular flow. The liquid-vapour interface in annular flow is nearly always characterised by surface waves due to high speed vapour flowing over it.

At higher vapour velocities, the crests of the waves of the liquid films are sheared off by the vapour flow and entrained in the core in the form of liquid droplets. This is referred to as the annular-mist flow regime because of the appearance of an annular film with a mixture of vapour and mist in the core flow.

At low void fractions slug flow is formed when interfacial waves grow sufficiently in amplitude to block the entire cross section at some axial locations, leading to the visual appearance of slug of liquid flowing down the tube. These slugs create large pressure spikes, due to rapid deceleration of the vapour flow. In other cases, flow that would visually be identified as slug flow does not create these large pressure spikes. This regime has been designated as pseudo-slug flow. It is proposed that unlike true slugs, pseudo-slugs either did not entirely block the tube or did so only momentarily.

As condensation continues, the slugs coalesce into a predominantly liquid flow with large bubbles. This is referred to as the plug flow regime. Turbulent fluctuations within the liquid eventually break these plugs into smaller vapour bubbles that become dispersed throughout the liquid. This is called the bubbly flow regime. The slug, plug and bubbly flow regimes occur at the end of the condensation process when the liquid inventory is large (the void fraction is small). In combination they occupy only 10 to 20% of the total quality range. The plug and bubbly flow regimes are confined to the bottom of the quality range; here the vapour mass fractions and consequentially the energy transfer rates due to condensation are negligibly small. The heat transfer rates should be estimated on the basis of single-phase liquid flow.

Since the flow pattern strongly influence the heat and momentum transfer processes, it is important for designers to predict what flow pattern is expected based on the flow rate, quality, fluid properties, and tube diameter. One of the earliest attempts at flow regime map was by Baker [7]. The Baker map was based on observations of adiabatic gas-liquid flows in tube ranging from 25.4 to 101.6 mm in diameter. The data used included both air-water and oil-water flows, providing a fairly wide range of fluid properties. The horizontal and vertical coordinates on the Baker's map are the superficial liquid and vapour mass fluxes, times scaling factors, that account for fluid property variations. Although subsequent flow regime maps have achieved improved accuracy, Baker's work is historically the first widely recognized flow regime map.

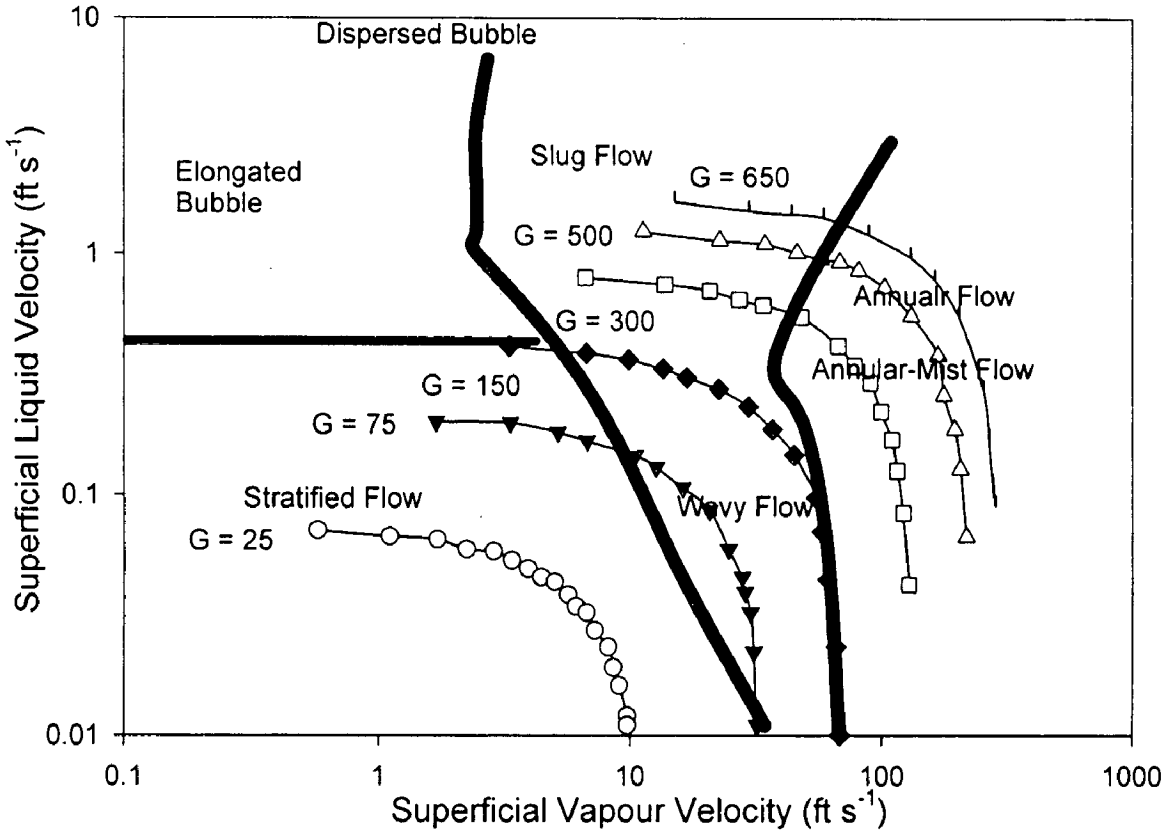

Fig. 2.2 Flow pattern prediction for R-134a at 45°C by the map of Mandhane et al. [9].

Mandhane et al. [9] developed a flow regime map similar to Baker's [7] using a larger database. The abscissa and ordinate of the Mandhane map are superficial gas velocity and superficial liquid velocity, which makes it rather simple to use. Their map correctly

predicted the flow regime for 68 percent of the observations in their database, as opposed to 42 percent for the original Baker map. One of the most theoretically based flow regime map is that of Taitel and Dukler [6], they reasoned that each flow regime transitions was based on a different set of competing forces and that a single parameter or set of coordinates should not be expected to predict all flow regime transitions. Their map includes five flow regimes; stratified smooth, stratified-wavy, annular, intermittent and dispersed bubble. They developed various approaches for predicting the transitions between the various flow regimes based on the appropriate physical mechanisms. For the stratified to wavy flow transition, they hypothesised that waves would be formed when the pressure and shear forces acting on a wave were sufficient to overcome viscous dissipation in the wave.

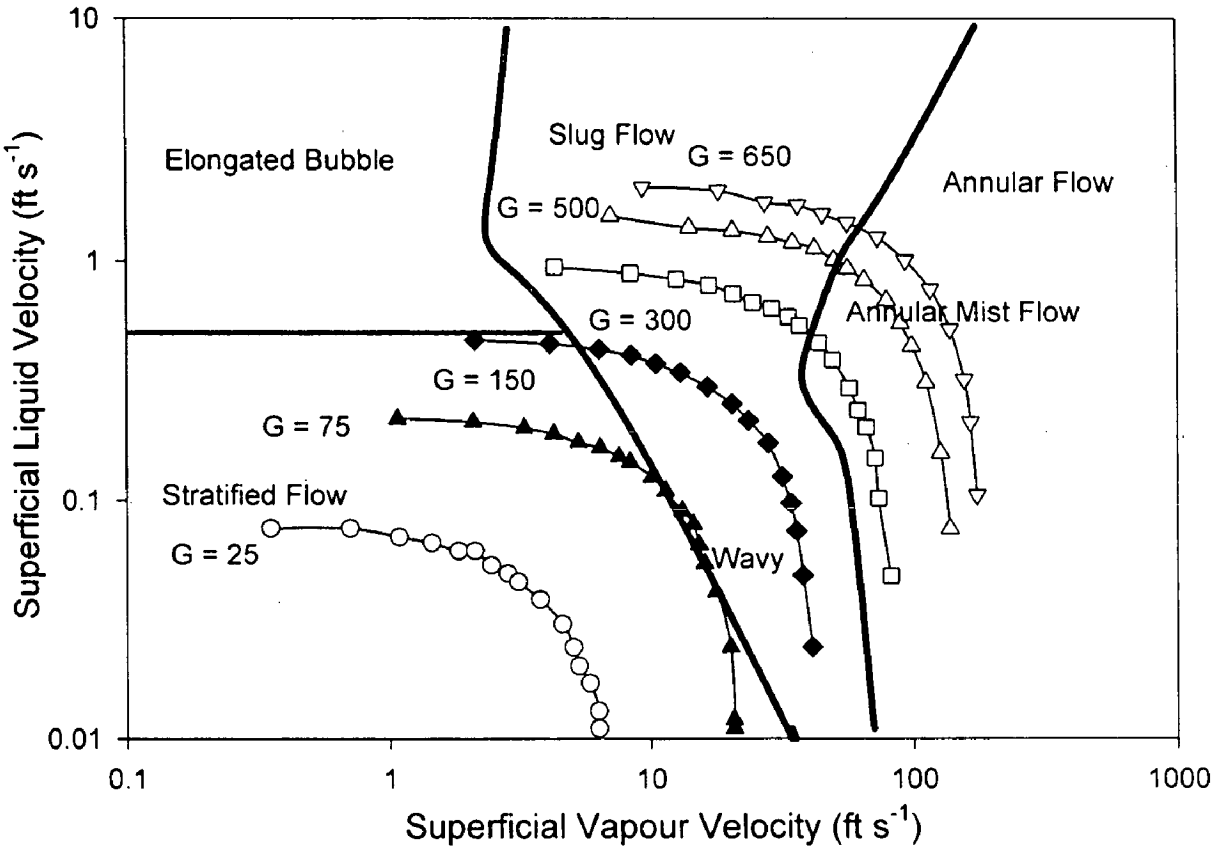

Fig. 2.3 Flow pattern prediction for R-32/R-125 at 45°C by the map of Mandhane et al. [9].

Another approach to predicting flow regime transitions, specifically for condensation, has been developed by Soliman [17]. He distinguished between three flow regime that he deemed to be important for condensing flows; wavy flow, annular flow, and mist flow.

He developed two flow regime transition criteria, one for the wavy to annular transition and one for the annular to mist transition. It is important to note that the wavy flow regime of Soliman includes the regimes commonly called stratified, slug, and wavy flow. While these regimes have important differences from the standpoint of flow regime classification, particularly concerning the stability of the wavy interface, He concluded that these differences were less important than the significant stratification that they all had in common.

Soliman [17] postulated that the wavy to annular transition was based on a balance between inertial and gravitational forces acting on the liquid film. The Froude number, V^2/gL, represents a balance between these forces. He proposed that the appropriate velocity was the actual liquid velocity and the appropriate length scale was the film thickness. These parameters were not known based solely on mass velocity, vapour quality, and the fluid properties. Soliman obtained expression for them based on relations for two phase pressure drop in annular flow. Thus, his transition criterion is opposite to that of Taitel and Dukler [6] in that it assumes that an annular flow exists and seeks to determine when gravitational forces will cause a transition to wavy flow.

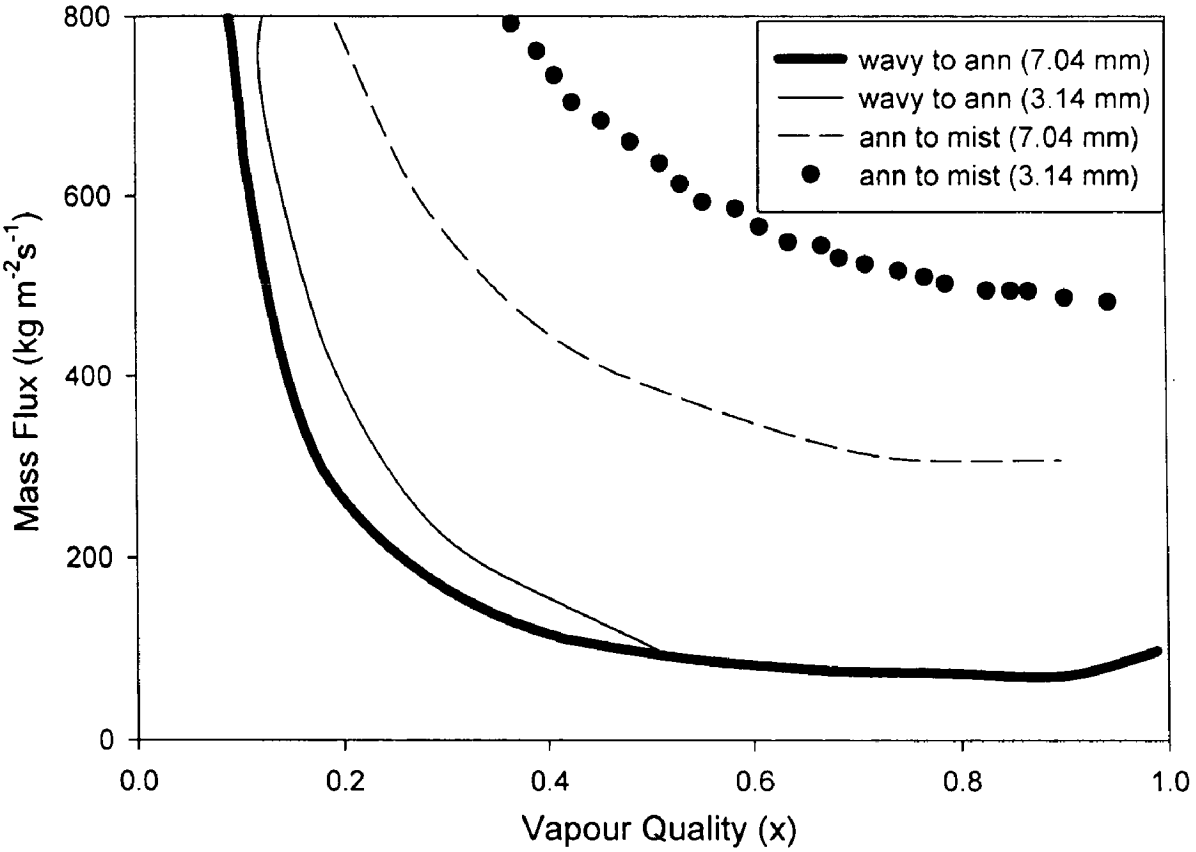

Fig. 2.4 Flow pattern prediction for R-134a at 35°C by the map of Soliman [17].

Based on comparison with data in tubes of 4.8 mm to 25 mm in diameter, and with fluids including water, refrigerants, and acetone, Soliman [17] concluded that wavy flow was observed for $Fr_{so} < 7$, and annular flow was observed for $Fr_{so} > 7$. Dobson and Chato [16] reported that for $Fr_{so} = 7$ served as a good indicator of the transition from wavy to wavy-annular flow, although a symmetric annular flow was not observed until around $Fr_{so} = 18$.

Soliman [17] also developed a parameter for predicting the transition from annular to mist flow. He postulated that the primary forces tending to prevent entrainment were liquid viscous forces and surface tension forces, and that the primary force which promoted was vapour inertia. He formulated a modified Weber number that represented a balance between these forces. Soliman concluded that the annular flow was always observed for $We_{so} < 20$, and pure mist flow with no stable liquid film on the wall was always observed for $We_{so} > 30$. The region of We_{so} between 20 and 30 was reported to be a mix of annular and mist flow, called annular-mist flow.

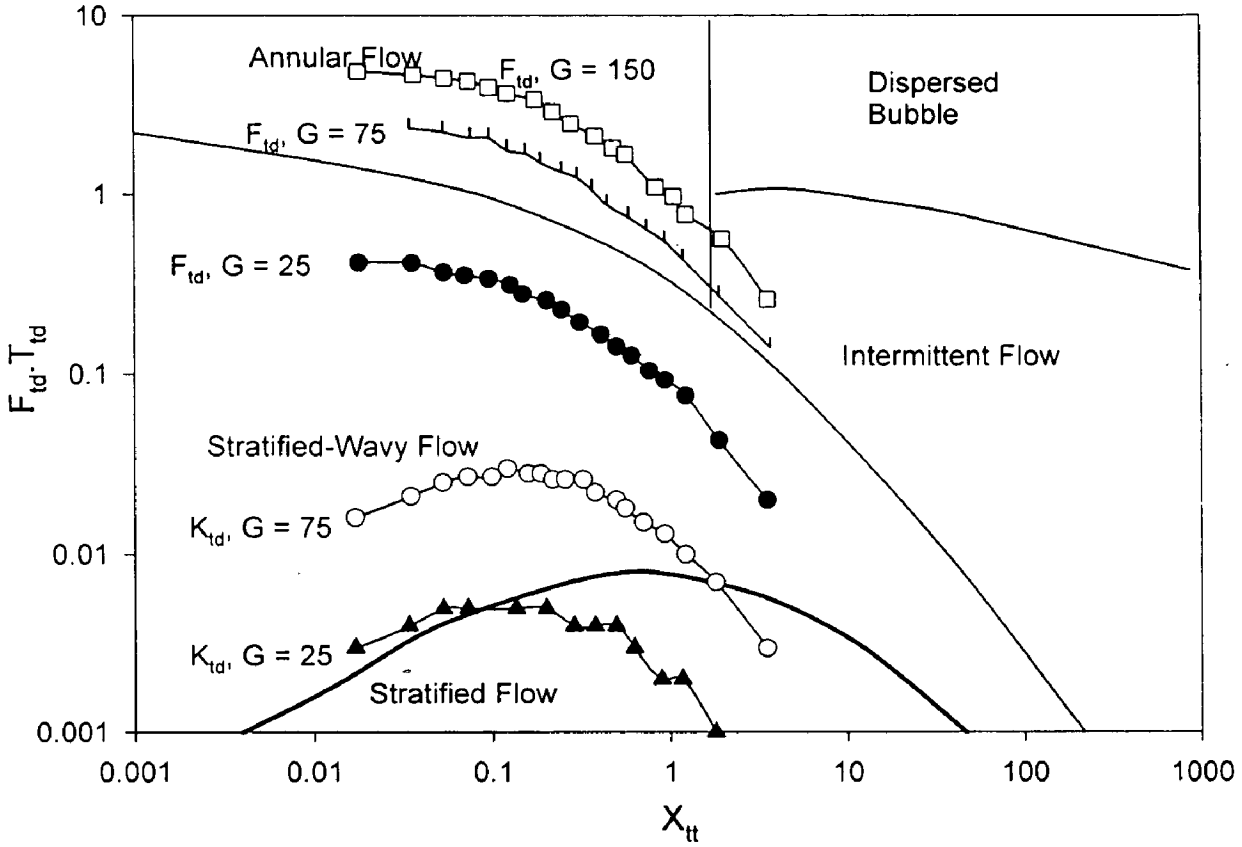

Fig. 2.5 Flow pattern prediction for R-134a at 35°C in a 7.04 mm tube by the map of Taitel and Dukler [6].

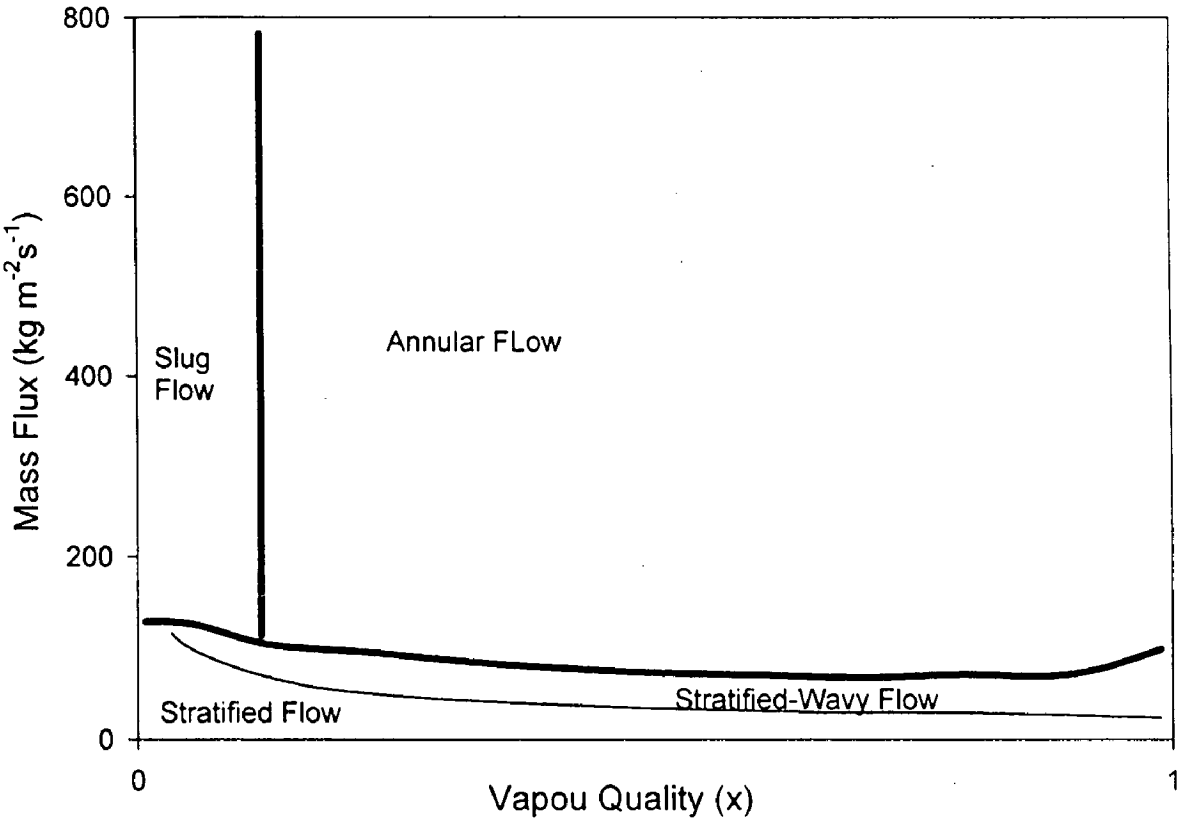

Fig. 2.6 Flow pattern prediction for R-134a at 35°C in a 7.04 mm tube by the map of Taitel and Dukler [6].

Dobson and Chato [16] presented the experimental flow regime observation and compared them to various flow regime predictors from the literature. There observations were gathered in tubes of 3.14, 4.57, and 7.04 mm inner diameters. The refrigerants used were R-134a, R-22, and 60/40 and 50/50 blends of R-32 and R-125. The dominant factors affecting the flow regime were the mass flux and the quality. At the lowest mass flux in the study 25 kg $m^{-2}s^{-1}$, smooth stratified flow was observed across the entire range of quality. As the mass flux was increased to 75 kg $m^{-2}s^{-1}$, interfacial waves developed and wavy flow was observed for the entire range of quality. For these two mass fluxes, the flow regime was not affected by changes in diameter or refrigerant.

At mass fluxes of 150 and 300 kg $m^{-2}s^{-1}$, several different flow regimes were observed as the quality was changed. Slug flow was observed at low qualities, followed sequentially by wavy, wavy-annular, and annular flow. At these mass fluxes, the tube diameter and fluid properties influenced the range of quality over which each of the flow regimes occurred. At the highest mass fluxes in their studies, 500, 650, 800 kg $m^{-2}s^{-1}$, the flow

regimes included slug flow at low quality, followed by wavy-annular and annular-mist flow as the quality was increased. Although the quality range over which each of these regimes occurred depended somewhat on fluid properties and diameter, annular or annular-mist flow normally occurred for the 70 to 80 percent of the condensation path. These were the only mass fluxes where significant entrainment occurred. Perhaps the most significant observation of their studies high mass flux was that pure mist flow (without a stable wall film) was observed only at qualities over 90 percent, and even then never at the outlet sight glass.

Tandon et al. [11] presented the results of an experimental investigation on heat transfer behaviour during forced convection condensation inside a horizontal tube for wavy, semi-annular and annular flows. A qualitative study was made of the effect of various parameters – refrigerant mass flux, vapour quality, condensate film temperature drop and average vapour mass velocity- on average condensing heat transfer coefficient. Ackers-Rosson [13] correlations with changed constant and power have been recommended for the two flow regimes.

2.2 MODELS FOR CONDENSATION INSIDE SMOOTH TUBES

Heat transfer during condensation inside horizontal plain tubes has been widely studied in the past, both experimentally and theoretically. Many data sets are available for condensation. Some of the previous models, which were widely accepted at that time, are discussed here.

2.2.1 Jaster and Kosky Model (1976)

Jaster and Kosky [18] have established a single value criterion for the transition in flow regime between annular and stratified flow. A correlation of the transition between annular flow and stratified flow is made in terms of the stress ratio F, where

F = (axial shear force)/ (gravitational body force)

$$F = \frac{\tau_w}{\rho_l g \delta} \tag{2.1}$$

In this correlation a basic problem was to discover a convenient form to express τ_w and δ in terms of the accessible flow parameter of the system, data taken under condensation in the annular, transitional and stratified flow regime and compared, it is observed that the value of F is clear indicator of the flow regime. Annular flow was observed for $F > 29$, and for $F < 5$ it was stratified flow, with the transition flow for $5 < F < 29$.

In fully annular regime the heat transfer through the flowing film is governed by boundary layers:

$$N_{an} = \frac{1}{T^+} \frac{\rho_L D C_{pl} \mu}{K_l} \tag{2.2}$$

For fully stratified flow previous correlations are very convenient to use. A simplification is given which assumes that heat transfer through the accumulated condensed flow is negligible compared to the film condensation in the upper portion of the tube. A flat draining liquid level is assumed and the correlation for fully stratified flow regime is given

$$N_{str} = \frac{0.725D}{K_L}\left[\frac{K_L^3 \rho_L (\rho_L - \rho_V) h_{fg} g}{\mu_L D \Delta T_s}\left(\frac{1+\cos B}{2}\right)^3\right]^{1/4} \quad (2.3)$$

Where β is the half angle subtended at the centre of the tube by the chord formed at the surface of the draining film. Based on this a Nusselt number correlation is proposed for the transitional flow as

$$N_{tr} = N_{an} + \frac{F-29}{24}(N_{an} - N_{str}) \quad (2.4)$$

Using steam/water data values of F were measured at the boundaries of the transitional flow regime. These experiments did not indicate a flow regime dependence on L/D ratio, the small range of L/D actually tested, limits this conclusion. The tested range was 173 > L/D > 136. They also did not distinguish between turbulent and annular flow as specified on a simple Re_v basis. The heat transfer in the mixed flow regime was correlated in terms of Nusselt number compared as a linear function of the stress ratio.

2.2.2 Shah Model (1979)

Shah [14] has presented a simple dimensionless correlation for predicting heat transfer coefficient during film condensation inside pipe. It has been verified by comparison with a wide variety of experimental data. These include fluid water, R-11, R-12, R-22, R-113, methanol, ethanol, benzene and trichloroethylene condensing in horizontal, vertical and inclined pipes of diameter ranging from 7 to 40 mm. Four hundred and seventy four data points representative of much greater number, from 21 independent studies have been correlated with a mean deviation of about 15 percent.

For the two-phase flow the heat transfer coefficient given by Shah is

$$h_{TP} = h_L\left[(1-x)^{0.8} + \frac{3.8x^{0.76}(1-x)^{0.04}}{P_r^{0.38}}\right] \quad (2.5)$$

where h_L is the heat transfer coefficient for the liquid phase. The mean heat transfer coefficient is calculated as

$$h_{TPM} = \frac{1}{L}\left[\int_0^L h_{TPL}\, d_L\right] \quad (2.6)$$

Quite a few of the measurement at vapour qualities 85% to 100% were found to be substantially higher than predictions. One explanation could be the entrances; as such high qualities generally prevail near the entrance. Another possibility could be that the vapour shear may be so high as to cause high entrainment or even breakdown of a continuous liquid film. The accuracy of correlation seems to decrease with decreasing Reynolds number. However the data for $Re_L > 3000$ are quite well correlated.

2.2.3 Dobson and Chato Model (1998)

Dobson and Chato [16] have tested the refrigerants R-22, R-12, R-134a, and near azeotropic blends of R-32/R-125 in various compositions. The study focused primarily on measurement and prediction of condensing heat transfer coefficient and the relationship between heat transfer coefficient and two phase flow regime.

They observed flow regimes with R-134a, R-22 and nearly azeotropic mixtures of R-32/R-125 condensing inside tubes having 3.1 mm, 4.6 mm and 7.1 mm inside diameter. At mass velocity 'G' of 24 kg $m^{-2}s^{-1}$ smooth stratified flow was observed over the entire quality range, at mass velocity of 75 kg $m^{-2}s^{-1}$ wavy flow was observed at every quality tested, at G = 150 to 300 kg $m^{-2}s^{-1}$ annular flow was observed at high quality, followed sequentially, as vapour quality decreased, by wavy-annular (waves wet the tube circumference without symmetric annular flow), wavy and slug flow. At the highest flow rates tested (500, 645, 794 kg $m^{-2}s^{-1}$) the flow regimes included annular-mist at high quality, followed by annular, wavy-annular, and slug, as the quality decreased. They observed that, at constant saturation temperature and specific mass flow rate, the transition from wavy-annular flow to wavy flow and the transition from annular to wavy-annular flow shifted to lower qualities, as the tube diameter was reduced.

Flow regimes were observed visually at inlet and outlet of test condenser as the heat transfer data were collected. Annular, stratified-wavy, stratified, mist and slug flows were observed. The experimental results were compared with existing flow regime maps and some correlations were suggested. The heat transfer behaviour was controlled by prevailing flow regime. For the purpose of analyzing heat transfer behaviour, the flow regimes were divided into two broad categories of gravity-dominated and shear-dominated flows. In the gravity-dominated flow regime the dominant heat transfer mode

was laminar film condensation in the top of the tube. This regime was characterized by the heat transfer coefficients that depend on the wall to refrigerant temperature difference but were nearly independent of mass flux. In the shear dominated flow regime, forced convective condensation was the dominant heat transfer mechanism. This regime was characterized by the heat transfer coefficients that were independent of temperature difference but very dependent on mass flux and quality.

The heat transfer coefficient during annular flow, was calculated as

$$Nu = 0.023\,\mathrm{Re}_L^{0.8}\,\mathrm{Pr}_L^{0.4}\left[1+\frac{2.22}{X_{tt}^{0.89}}\right] \tag{2.7}$$

and for wavy flow:

$$Nu = \frac{0.23\,\mathrm{Re}_{vo}^{0.12}}{1+1.11X_{tt}^{0.58}}\left[\frac{Ga\,\mathrm{Pr}_l}{Ja_l}\right]^{0.25}+\left(1-\frac{\theta_L}{\pi}\right) \tag{2.8}$$

The flow regimes were defined by the modified Froude number and Weber number as discussed earlier. The modified Froude number is given by

$$Fr_{SO} = 0.025\,\mathrm{Re}_l^{1.59}\left(\frac{1+1.09X_{tt}^{0.039}}{X_{tt}}\right)^{1.5}\frac{1}{Ga^{0.5}} \quad \text{for } \mathrm{Re_l} \le 1250 \tag{2.9}$$

$$Fr_{SO} = 1.26\,\mathrm{Re}_l^{1.04}\left(\frac{1+1.09X_{tt}^{0.039}}{X_{tt}}\right)^{1.5}\frac{1}{Ga^{0.5}} \quad \text{for } \mathrm{Re_l} > 1250 \tag{2.10}$$

The modified Weber number is given by

$$We_{SO} = 2.45\frac{\mathrm{Re}_g^{0.64}}{Su_g^{0.3}(1+1.09X_{tt}^{0.039})^{0.4}} \quad \text{for } \mathrm{Re_l} \le 1250 \tag{2.11}$$

$$We_{SO} = \left[\left(\frac{\mu_g}{\mu_l}\right)^2\left(\frac{\rho_l}{\rho_g}\right)\right]^{0.084}\frac{\mathrm{Re}_g^{0.79}\,X_{tt}^{0.157}}{Su_g^{0.3}(1+1.09X_{tt}^{0.039})^{0.4}} \quad \text{for } \mathrm{Re_l} > 1250 \tag{2.12}$$

Here

$$Ga = \frac{g\rho_l(\rho_l - \rho_g)D_g^3}{\mu_l^2} \tag{2.13}$$

$$Ja_l = \frac{c_{p,l}(T_{sat} - T_w)}{i_{lg}} \tag{2.14}$$

2.2.4 Tandon et al. Model (1982)

Tandon et al. [11] have conducted test for heat transfer during forced convection condensation inside horizontal tubes, the test condenser consisted of three copper tube-in-tube test sections connected in series through visual section and mounted horizontally. Each test section was 1 m long and the inner tube I.D. was 10 mm and O.D. 12.5 mm. The outer tube was also of copper of 50 mm I.D. The system was designed to obtain average condensing heat transfer coefficient of each test section. To visualize flow patterns four sight glass tubes were provided. These were also of I.D. 10 mm necessary arrangements were made to measure tube wall, refrigerant and cooling water temperature at appropriate points. Refrigerant pressure, coolant flow rate and refrigerant flow rate were also recorded.

They tested refrigerants R-12 and R-22, and presented a modified Ackers-Rosson [13] correlation.

For shear controlled flows (annular and semi annular):

$$Nu = 0.084\ (Pr_L)^{1/3}\ (h_{fg}/C_P\Delta T)^{1/6}\ Re_V^{0.67} \qquad \text{for } Re_V > 30000 \tag{2.15}$$

For gravity controlled flow (wavy flow):

$$Nu = 23.1\ Pr_L^{1/3}\ (h_{fg}/C_P\Delta T)^{1/6}\ Re_V^{1/8} \qquad \text{for } Re_V < 30000 \tag{2.16}$$

For $Re_V = 30000$ the changeover of flow from annular and semi annular flow to wavy flow was observed.

2.2.5 Sarma et al. Model (2002)

Sarma et al. [19] employed homogeneous model approach in the estimation of shear velocity, which was subsequently, made use of in predicting local convective condensation heat transfer coefficients. The resulting analysis of their study was

compared with some of the available equations in the literature. It was observed that the agreement is reasonably satisfactory validating the assumptions and the theory presented. The condensations of vapours irrespective of the type of flow regime in the condenser tube were treated as a homogeneous model under adiabatic conditions with heat removal. In single-phase convective problems related to either heating or cooling of the medium without phase change, it is established that modified Reynolds analogy with correction for Prandtl number variation responds favourably and the heat transfer coefficients can be predicted from the momentum transfer analysis.

The temperature gradients at the wall for single-phase turbulent flow conditions were approximately close to those at the wall for two-phase flow in as much as the wall is always wetted by the condensate and the influence of the hydrodynamic regime in the core can exert marginal influence on the heat transfer rate.

Sarma et al. [19] has given the ratio of Nusselt number for the two-phase flow and for the liquid phase as:

$$\frac{Nu_{T.P}}{Nu_L} = C_3\phi_L \tag{2.17}$$

where $Nu_L = 0.023\,\mathrm{Re}^{0.8}\,\mathrm{Pr}^{0.4}(1-x)^{0.8}$ (2.18)

So the convective condensation heat transfer for the two-phase is given by the following equation:

$$Nu_{T.P} = 0.023C_3\phi_L\,\mathrm{Re}^{0.8}\,\mathrm{Pr}^{0.4}(1-x)^{0.8} \tag{2.19}$$

where $\mathrm{Re} = \dfrac{4m}{\pi D\mu_L}$ and (2.20)

$$\phi_L^2 = \frac{\Delta P_{T.P.F}}{\Delta P_{L.P.F}} \tag{2.21}$$

where ϕ_L is the friction multiplier as defined by Lockhart and Martinelli parameter.

2.2.6 Boissieux et al. Model (2000)

Boissieux et al. [20] presented their results of condensation of refrigerants Isceon-59, R-407C and R-404a in a horizontal smooth tube. They have compared their results with correlation of Shah's [15] and that of Dobson and Chato [16].

The Dobson and Chato [16] correlation predicts well the results for vapour quality below 70% but it seems to over predict the experimental data at higher qualities. It was found that experimental data were higher than the calculated ones at low vapour qualities because of the higher heat flux during some of experiments. A good prediction was found by Shah's [15] correlation between 0 to 60 percent vapour quality, but the correlation over predicts the heat transfer coefficient at higher vapour quality. This probably occurs because this correlation has been developed for pure refrigerant and the experimental results presented here were for zeotrope refrigerant mixtures.

The Shah [15] correlation for condensation heat transfer coefficient was found to predict adequately the local experimental results with an overall standard deviation of 9.1 percent. The Dobson and Chato [16] correlation gave the best prediction of the three refrigerant considered in this study, with an average standard deviation of 7.6 percent.

2.2.7 Cavallini et al. Model (2001)

Cavallini et al. [21] measured local heat transfer coefficients and pressure drops during condensation of refrigerants R-22, R-32, R-125, R-410A, R-236ea, R-134a, R-407C within a horizontal 8 mm inside diameter tube, in wide ranges of mass velocities, saturation temperatures, vapour qualities and temperature differences (T_s-T_w). They confirmed that, during condensation of pure fluids and nearly azeotropic mixtures, in the annular flow regime the heat transfer coefficient varies with mass velocity G, vapour quality x and saturation temperature; only in the stratified regimes the measured heat transfer coefficient was affected by temperature difference between saturation and tube wall (T_s-T_w). Since flow regimes strongly influence the heat and momentum transfer processes, any sound prediction of two-phase heat transfer during condensation must be based on the analysis of the occurring flow pattern. The heat transfer behaviour depends on the flow regime and particularly on the relative importance of inertial and gravitational forces on the liquid film.

2.2.8 Cavallini et al. Model (2002)

Cavallini et al. [12] presented a computational method, which is based upon a large data bank, is used for condensation of halogenated refrigerants inside tubes with internal diameter d > 3 mm, at reduced pressure Pr < 0.75 and density ratio ($\rho_L/\ \rho_G$) > 4. For annular flow it starts from the theoretical model by Kosky and Staub [23], where the heat transfer coefficient is correlated to the frictional pressure gradient through the interfacial shear stress. A new equation, based on the Friedel parameters, was obtained for the frictional pressure gradient during annular flow, to be used for calculating the interfacial shear stress. The model is based on the map on the boundary of the flow regime regions on a mass velocity and vapour quality chart; in this representation, a complete condensation process follows a horizontal line.

When the dimensionless vapour velocity gets lower than 2.5 and the Martinelli parameter $X_{tt} < 1.6$, the flow enters the annular-stratified flow transition and stratified flow region. The heat transfer coefficient between annular flows to stratified flow is then calculated from a linear interpolation between the heat transfer coefficient at the boundary of the annular flow region and that for fully stratified flow. In stratified flow, at very low value of dimensionless vapour velocity, heat is transferred in the upper part of the tube through a thin gravity driven film and, in the lower part of the tube, through a thick liquid film. The heat transfer coefficient for fully stratified flow is thus expressed as the sum of two components: the first component is calculated from a Nusselt type equation and is relative to the upper part of the tube; the second component is given as a convective term and refers to the lower part of the tube. This last term is not negligible at high values of reduced pressure. In this term the heat transfer coefficient of the liquid is multiplied by the fraction of surface area ($1-\theta/\pi$), while the first term refers to θ/π and the dependence on θ/π is expressed in terms of vapour quality.

When Martinelli parameter X_{tt} gets larger than 1.6, with dimensionless vapour velocity less than 2.5, the flow enters the stratified-slug transition and slug flow pattern region. Cavallini et al. [21] provided an empirical equation fitted from experimental data taken during slug flow. However, this equation for the slug flow region is not tuned to the heat transfer coefficient computed with the equations for stratified flow leading in some cases

to an abrupt variation of the heat transfer coefficient when varying vapour quality or mass velocity. Therefore, when $X_{tt} > 1.6$ and dimensionless vapour velocity is less than 2.5 it is suggested here that the heat transfer coefficient be computed as a linear interpolation between the coefficient computed at $X_{tt} = 1.6$ and the one for the liquid flowing with the entire flow rate. For the direct transition from annular to slug flow, that should occur at dimensionless vapour velocity equals to 2.5 and $X_{tt} > 1.6$, no experimental data are available. In fact, that transition occurs at very high mass velocity ($G > 1000$ kg $m^{-2}s^{-1}$ for the usual halogenated refrigerants) and low vapour quality, depending on the fluid and operating conditions. However, at that boundary the heat transfer coefficient may be linearly prorated down to heat transfer coefficient of gas phase with total flow rate, with respect to vapour quality x. Heat transfer coefficients have been calculated with the Cavallini et al. [21] model for condensation of R-134a, R-22, R-410A and R-32 in a 8 mm plain tube, and compared against the predictions of Shah [15] model, and the model by Dobson and Chato [16]. The given validity ranges of the different models have been accounted for and accordingly some models could not be applied at all operating conditions. The Cavallini et al. [21] model gives more conservative heat transfer coefficients compared with the other correlations, above all with respect to the high pressure refrigerants R-410A and R-32, for which both the Shah [15] and Dobson-Chato [16] models severely overestimate the experimental values.

The heat transfer model equation by Cavallini et al. [12] is given as:

For annular flow when dimensionless vapour velocity is more than 2.5

$$\alpha = \alpha_{an} = \rho_L c_{pL} \left(\frac{\tau}{\rho_L} \right)^{0.5} / T^{+} \tag{2.22}$$

for annular-stratified flow to be applied when dimensionless velocity is less than 2.5 and the Martnelli parameter is less than 1.6 is given by

$$\alpha = \alpha_{an-st} = (\alpha_{an,JG=2.5} - \alpha_{st})(JG / 2.5) + \alpha_{st} \tag{2.23}$$

and for stratified flow and slug flow when the dimensionless velocity is less than 2.5 but the Martinelli parameter is greater than 1.6,

$$\alpha = \alpha_{st-st} = \alpha_{LO} + x(\alpha_{1.6} - \alpha_{LO}) / x_{1.6} \tag{2.24}$$

$$\text{here } x_{1.6} = \left(\frac{\mu_L}{\mu_G}\right)^{1/9}\left(\frac{\rho_G}{\rho_L}\right)^{5/9} \Big/ \left[1.686 + \left(\frac{\mu_L}{\mu_G}\right)^{1/9}\left(\frac{\rho_G}{\rho_L}\right)^{5/9}\right] \tag{2.25}$$

Data points have been conventionally subdivided among high, middle and low-pressure refrigerants, considered at the same saturation temperature. It was observed that the prediction by the Dobson and Chato [16] model is unsatisfactory for the "high pressure" fluids (R-125, R-32, R-410A and R-32/R-125 60/40% by mass) at high values of the Nusselt number.

The available experimental data was compared against other widely used predictive semi-empirical procedures in Cavallini et al [21]. It was concluded that the Shah [15] correlation, very simple and much used for design of condensers, tends to over predict data relative to high pressure fluids, showing also too limited applicability ranges in this case.

Heat transfer through the thin film is usually analyzed by the classical Nusselt [22] theory as firstly suggested by Jaster and Kosky [18]. They neglected the heat transfer that occurs in the liquid pool at the bottom of the tube. As discussed by Dobson and Chato [16] this assumption is reasonable at very low mass velocities, but heat transfer in the liquid pool might not be negligible at high mass velocity and low quality, where wavy or stratified flow could prevail with substantial convective heat transfer in the bottom part of the tube. Cavallini et al. [21] compared experimental data taken in stratified flow against the predictions by the Jaster and Kosky [18] equation, and found an unsatisfactory agreement with available experimental data.

Chapter 3

IDENTIFICATION AND ANALYSIS OF TWO-PHASE FLOW REGIMES

3.1 LOGARITHMIC MEAN VOID FRACTION

For determining the transition between different two-phase flow regimes and to obtain the range of mass velocity at which a particular flow regime will prevail, void fraction is the most important parameter. Also to predict the two-phase heat transfer coefficient and two-phase pressure drop based on the flow patterns transition, void fraction prediction is the foremost parameter. Therefore it is important to have a method that is both accurate and reliable over the whole range of mass velocities, flow regimes and reduced pressures.

A number of void fraction models exist for the prediction of the cross sectional void fraction of a vapour in two-phase flow in a tube, which is defined as the cross sectional area occupied by the vapour with respect to the total cross-sectional area of the flow channel. Mostly accepted prediction methods for void fraction are as follows:

(1) **Homogeneous model:** in this model of void fraction prediction, it is assumed that both the phases; liquid phase and vapour phases travel at nearly the same velocity, such as near the critical point or at very high mass velocities where the flow regime is either the bubbly flow or the mist flow. At very high reduced pressure, the density of the vapour approaches that of liquid, at which point the homogeneous model is applicable.

The homogeneous void fraction is calculated as

$$\varepsilon_h = \left[1 + \left(\frac{1-x}{x}\right)\left(\frac{\rho_V}{\rho_L}\right)\right]^{-1} \tag{3.1}$$

(2) **One dimensional models:** in these models, one of the parameters, such as momentum or kinetic energy is minimized.

(3) **Drift flux models:** these are based on the radial velocity distribution in the two phases. Drift flux models are particularly attractive because they account for the

velocity distribution in the vapour and liquid phases and hence include the effect of mass velocity on void fraction.

There also exist some void fraction prediction models which are developed for particular flow regimes and are specific. Some models based on empirical methods are also available.

Of the numerous non-homogeneous void fraction models available Kattan et al. [3] chose the drift flux model of Rouhani and Axelsson [24] for their flow boiling model over others because drift flux models are more complete in describing the flow and include the effects of mass velocity and surface tension on void fraction.

The void fraction model given by Rouhani and Axelsson [24] is

$$\varepsilon_{RA} = \frac{x}{\rho_V}\left(\left[1+0.12(1-x)\right]\left[\frac{x}{\rho_V}+\frac{1-x}{\rho_L}\right]+\frac{1.18(1-x)\left[g\sigma(\rho_L-\rho_V)\right]^{0.25}}{G\rho_L^{0.5}}\right)^{-1} \tag{3.2}$$

They have found this void fraction equation to be particularly effective for pressure at low to medium range. The predictions for high pressure were not effective unlike those by homogeneous void fraction models when the pressure approaches to the critical. It is observed that the effect of pressure is not correctly accounted for by either of the two void fraction expressions. It is important to have a void fraction model equation that is valid over the entire range of reduced pressure. Therefore several approaches were investigated on how to best interpolate between the values of ε_h and ε_{RA}. A simple logarithmic mean between the values of ε_h and ε_{RA} was found to give the best results, where the logarithmic mean void fraction is defined as

$$\varepsilon = \frac{\varepsilon_h - \varepsilon_{RA}}{\ln\left(\frac{\varepsilon_h}{\varepsilon_{RA}}\right)} \tag{3.3}$$

This new void fraction expression was observed to predict better than the previous void fraction models and it is valid from low pressure up to those approaching the critical pressure, in terms of reduced pressure from 0.02 to 0.8, based on the comparison to the heat transfer data. In case of annular flow the convective heat transfer coefficient is very

sensitive to the void fraction prediction, as the liquid film Reynolds number is based on the mean velocity of liquid as

$$\mathrm{Re}_L = \frac{4G(1-x)\delta}{(1-\varepsilon)\mu_L} = \frac{Gd(1-x)}{\mu_L} \tag{3.4}$$

and the thickness of the liquid film can be calculated as

$$\delta = \frac{d(1-\varepsilon)}{4} \tag{3.5}$$

By the above relations the annular flow heat transfer coefficient is directly proportional to $(1-x)/(1-\varepsilon)$ where the value of void fraction is greater then that of vapour quality. In fact for, otherwise fixed conditions, the variation of convective condensation heat transfer coefficient versus vapour quality is dependent on the variation in void fraction. The slope of the curve between heat transfer coefficient and vapour quality is dependent on void fraction. It is therefore justifiable to utilize accurate annular flow condensation heat transfer data to select the most appropriate void fraction model in the absence of void fraction data at high reduced pressures.

3.2 LIQUID AND VAPOUR CROSS SECTIONAL AREAS

The cross sectional view of the tube can be presented by the figure given below

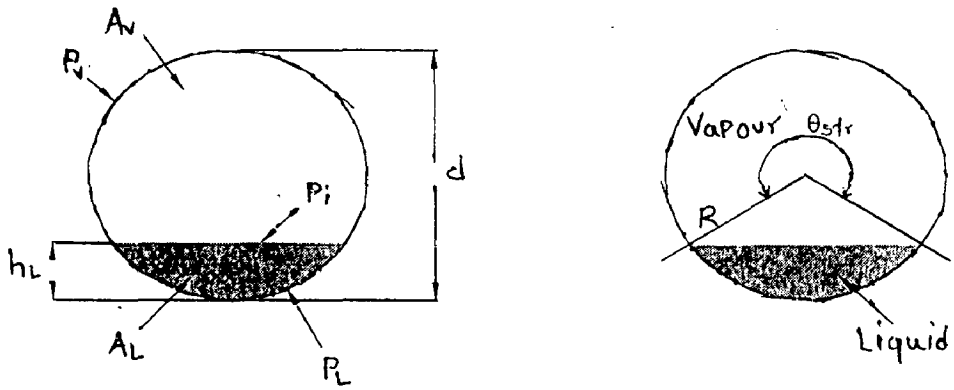

Fig. 3.1 Geometrical parameters for two-phase flow in a circular tube.

The cross sectional area A, of plain horizontal tube can be obtained by the geometry, based on void fraction the cross sectional area of both the phases; liquid and vapour can be calculated as:

$$A_{l,} = A(1-\varepsilon) \tag{3.6}$$

$$A_V = A\varepsilon \tag{3.7}$$

where A_L is the liquid phase and A_V is the vapour phase cross sectional area. The area A_L here ignores any liquid formed by film condensation on the upper perimeter of the tube. These cross sectional area are normalized using the tube internal diameter d to obtain the dimensionless variables:

$$A_{l,d} = \frac{A_{l,}}{d^2} \tag{3.8}$$

$$A_{Vd} = \frac{A_V}{d^2} \tag{3.9}$$

here A_{Ld} is the dimensionless cross section area for the liquid phase and A_{Vd} is the dimensionless cross section area for the vapour phase.

3.3 LIQUID FILM HEIGHT AND LENGTH OF INTERFACE

As defined in the figure the h_L is the height of the liquid film and P_i is the length of the interface. The dimensionless height of liquid film can be given as

$$h_{l,d} = \frac{h_{l,}}{d} \tag{3.10}$$

and the length of interface

$$P_{id} = \frac{P_i}{d} \tag{3.11}$$

as they are normalised, using the tube inside diameter.

The dimensionless height of the liquid film can be obtained by the expression:

$$h_{l,d} = 0.5\left(1-\cos\left(\frac{2\pi-\theta_{str}}{2}\right)\right) \tag{3.12}$$

and for the dimensionless length of interface:

$$P_{id} = \sin\left(\frac{2\pi - \theta_{str}}{2}\right) \tag{3.13}$$

where θ_{str} is stratified angle as shown in the figure.

3.4 THE STRATIFIED ANGLE

For fully stratified flow the angle on the cross section of the tube, called stratified angle can be obtained iteratively by the expression based on the dimensionless cross sectional area of the liquid phase;

$$A_{Ld} = \frac{1}{8}\left[(2\pi - \theta_{str}) - \sin(2\pi - \theta_{str})\right] \tag{3.14}$$

To completely avoid the iterative calculations, one expression given by Biberg [25] can be used. This expression is very accurate and the error involved in calculation of stratified angle by this expression is in the order of $5x10^{-5}$ for θ_{str} between 0 to 2π.

The implicit expression for the stratified angle is as:

$$\theta_{str} = 2\pi - 2\left\{\begin{array}{l} \pi(1-\varepsilon) + \left(\frac{3\pi}{2}\right)^{1/3}\left[1 - 2(1-\varepsilon) + (1-\varepsilon)^{1/3} - \varepsilon^{1/3}\right] \\ -\frac{1}{200}(1-\varepsilon)\varepsilon\left[1 - 2(1-\varepsilon)\right]\left[1 + 4((1-\varepsilon)^2 + \varepsilon^2)\right] \end{array}\right\} \tag{3.15}$$

This method avoids any iterative calculation and gives the stratified angle directly from the void fraction and has no effect on the location of the transition curves compared to the prior method.

3.5 MASS VELOCITIES FOR DIFFERENT FLOW REGIMES

Based on their experimental results Zurcher et al. [26] have given the expressions for mass velocities on the values of which different flow regimes prevail. The value of mass velocity at which the flow regime changes from stratified-wavy flow to fully stratified flow is calculated from the expression given as:

$$G_{str} = \left\{ \frac{(226.3)^2 A_{Ld} A_{Vd}^2 \rho_V (\rho_L - \rho_V) \mu_L g}{x^2 (1-x) \pi^3} \right\}^{1/3} + 20x \tag{3.16}$$

The flow will remain in the stratified flow regime for any value of mass velocity 'G' less than G_{str}.

The transition curve from stratified-wavy flow to intermittent flow and annular flow is given as:

$$G_{wavy} = \left\{ \frac{16 A_{Vd}^3 g d \rho_L \rho_V}{x^2 \pi^2 \left(1 - (2h_{Ld} - 1)^2\right)^{0.5}} \left[\frac{\pi^2}{25 h_{Ld}^2} (1-x)^{-F_1(q)} \left(\frac{We}{Fr} \right)_L^{-F_2(q)} + 1 \right] \right\}^{0.5} + 50 - 75 e^{-(x^2 - 0.97)^2 / x(1-x)} \tag{3.17}$$

In the above expression $F_1(q)$ and $F_2(q)$ are the non-dimensional empirical exponents accounting for the effect of heat flux on dryout during evaporation, and these are given as:

$$F_1(q) = 646.0 \left(\frac{q}{q_{crit}} \right)^2 + 64.8 \left(\frac{q}{q_{crit}} \right) \tag{3.18}$$

$$F_2(q) = 18.8 \left(\frac{q}{q_{crit}} \right) + 1.023 \tag{3.19}$$

where the critical heat flux q_{crit} was used to normalize the local heat flux. They have given these expressions first for boiling, and the heat flux effect on dryout is not required for condensation, hence q = 0. Thus, the values of F_1 and F_2 becomes 0 and 1.023, respectively for condensation and G_{wavy} for condensation becomes

$$G_{wavy} = \left\{ \frac{16 A_{Vd}^3 g d \rho_L \rho_V}{x^2 \pi^2 \left(1 - (2h_{Ld} - 1)^2\right)^{0.5}} \left[\frac{\pi^2}{25 h_{Ld}^2} \left(\frac{We}{Fr} \right)_L^{-1.023} + 1 \right] \right\}^{0.5} + 50 - 75 e^{-(x^2 - 0.97)^2 / x(1-x)} \tag{3.20}$$

the minimum value of mass velocity in stratified-wavy flow regime is called minimum mass velocity for this flow regime, $(G_{wavy})_{min}$ and the value of vapour quality at which the minimum mass velocity for this flow regime occurs is the minimum vapour quality for the flow regime. For all values of vapour quality more than the minimum the mass velocity is assigned the value of minimum mass velocity $(G_{wavy})_{min}$.

To differentiate between intermittent and annular flow regimes, a value of vapour quality x_{IA} is obtained using the Martinelli parameter. For turbulent flow of both the vapour and liquid phase, the boundary curve of the intermittent flow to annular flow is defined by Martinelli parameter X_{tt}, fixing a value of 0.34 as given below

$$X_{tt} = \left(\frac{1-x}{x}\right)^{0.875}\left(\frac{\rho_V}{\rho_L}\right)^{0.5}\left(\frac{\mu_L}{\mu_V}\right)^{0.125} \tag{3.21}$$

by extracting the vapour quality from the above equation, the boundary curve of the intermittent to annular flow in the new flow map is calculated by

$$x_{IA} = \left\{\left[0.2914\left(\frac{\rho_V}{\rho_L}\right)^{-1/1.75}\left(\frac{\mu_L}{\mu_V}\right)^{-1/7}\right]+1\right\}^{-1} \tag{3.22}$$

After the annular flow if the mass velocity is further increased, then the flow regime that prevails is the mist flow regime. For all the values of mass velocity more than G_{mist} the mist flow regime is prevailing. The value of G_{mist} is calculated by

$$G_{mist} = \left\{\frac{7680 A_{Vd}^2 g d \rho_L \rho_V}{x^2 \pi^2 \xi}\left(\frac{Fr}{We}\right)_L\right\}^{0.5} \tag{3.23}$$

it depends strongly on the ratio of liquid Froude number and liquid Weber number. Where the Weber number is the ratio of the inertia to the surface tension forces and the Froude number is the ratio of inertia to gravity forces.

$$\left(\frac{We}{Fr}\right)_L = \frac{g d^2 \rho_L}{\sigma} \tag{3.24}$$

and the factor ξ is

$$\xi = \left[1.138 + 2\log\left(\frac{\pi}{1.5 A_{Ld}}\right)\right]^{-2} \tag{3.25}$$

For mist flow regime the minimum value of mass velocity is find and set as the minimum mass velocity for this regime $(G_{mist})_{min}$. The value of vapour quality at which this $(G_{mist})_{min}$ occurs is set as the minimum value of mass velocity for this regime as x_{min}. For

all values of vapour quality greater than the minimum value of vapour quality x_{min} the value of mass velocity more than the minimum is set at the minimum value.

Bubbly flow occurs at very high mass velocities. The transition for bubbly flow is given as:

$$G_{bubbly} = \left\{ \frac{256 A_{vd} A_{ld}^2 d^{1.25} \rho_l (\rho_l - \rho_v) g}{0.3164(1-x)^{1.75} \pi^2 P_{id} \mu_l^{0.25}} \right\}^{1/1.75} \tag{3.26}$$

Based on the value of mass velocity obtained by the above expressions and the corresponding value of vapour quality, it can be predicted that which of the flow regime is prevailing at a specific flow condition of mass velocity and a particular saturation temperature.

More specifically we can say that, stratified flow exists if the value of mass velocity 'G' is less than the mass velocity at fully stratified flow condition i.e. $G < G_{str}$.

Stratified-wavy flow regime prevails if the mass velocity is in between the values of mass velocity at fully stratified flow and the value of mass velocity at wavy flow condition i.e. $G_{str} < G < G_{wavy}$.

Intermittent flow regimes exists if the fixed mass velocity is greater than that at stratified-wavy flow mass velocity and at the same time the vapour quality is less than that at transition from intermittent to annular flow regime i.e. $G > G_{wavy}$ and $x < x_{IA}$.

Annular flow regime exists if fixed mass velocity is greater than the mass velocity at stratified-wavy flow condition and vapour quality is more than that at intermittent to annular flow transition i.e. $G > G_{wavy}$ and $x > x_{IA}$.

Mist flow regime prevails if the fixed mass velocity 'G' is greater than the mass velocity at mist flow transition i.e. $G > G_{mist}$.

3.6 EFFECT OF VARIABLES ON FLOW PATTERN TRANSITION

The effects of various variables on the transition of flow pattern are discussed here under.

3.6.1 Mass Flux and Quality

A smooth stratified flow regime is expected if the mass velocity is very low or at the lowest, and this regime will prevail for the entire range of quality. As the mass flux is increased, interfacial waves develop and stratified-wavy flow regime occurs and exists for the entire range of quality.

At these very low mass velocities, we can say around less than 80 kg $m^{-2}s^{-1}$, the flow regime is not affected by the entire change in diameter or even the refrigerant. If we go on increasing the mass velocity, let's say around more than 125 kg $m^{-2}s^{-1}$ to around 400 kg $m^{-2}s^{-1}$, several different flow regimes occur as the vapour quality 'x' changes. Slug flow is found at low vapour qualities, followed sequentially by stratified-wavy flow, intermittent flow, and annular flow. At these mass fluxes, the tube diameter and fluid properties influence the range of quality over which each of the flow regimes occurred. At even higher mass fluxes the flow regimes include slug flow at low quality, followed by stratified-wavy flow, intermittent flow, and annular flow as the quality increases. At these high mass fluxes significant entrainment occurs, the magnitude of which tends to vary in time. A pure mist flow, without a stable wall film, is observed only at vapour qualities over 90% without condensation. Mist flow seems to develop a stable liquid film as soon as condensation begins.

3.6.2 Reduced Pressure and Fluid Properties

Mass flux and vapour quality are the most important factors affecting the flow regimes but the thermo physical properties of the fluid and the tube diameter are also very important. At the intermediate mass fluxes of around 100 to 400 kg $m^{-2}s^{-1}$ these parameters are very much important, as here the mass velocities are neither as high nor low as to allow one flow regime to clearly dominate over the other. The primary fluid properties that affect the flow regimes are the vapour and the liquid densities and

viscosities and the surface tension. The variations in the fluid properties are related to the value of reduced pressure. At high values of reduced pressure, the liquid and vapour phases are more similar. Thus vapour density and viscosity are higher, and liquid density and viscosity are lower. The surface tension that represents the work required to increase the interfacial area, also decreases as the reduced pressure increases and the phase become more similar.

The most noticeable effect of the property difference on the flow regimes is the extent to which annular flow prevails over stratified-wavy or intermittent flow. At a given mass flux where stratified-wavy flow, intermittent flow, and annular flow all occur, the size of the quality range occupied by annular flow is greater at lower reduced pressures. Reduced pressure also affects the length of the slug flow.

3.6.3 Tube Diameter

The tube diameter has a significant affect on the flow regime transitions and it is also an important parameter to decide that which flow regime is prevailing. As the tube diameter is reduced at a fixed mass flux, the transition from stratified-wavy flow to intermittent flow and intermittent flow to annular flow shifts to lower qualities. At high mass fluxes most of the quality range is associated with annular flow and the diameter effects are less pronounced.

If the ratio of length-to-diameters is very small then the flow regime prevails is the fully stratified floe regime. Entrainments can be expected only at high mass fluxes. Although estimating the amount of entrainment is difficult, it appears that entrainment is less pronounced in the smaller tubes. Surface tension forces become increasingly important, as the diameter is decreased and may dominate for sufficiently small tube sizes.

Chapter 4

TWO-PHASE HEAT TRANSFER MODEL

The development of condensation heat transfer model for the two-phase flow, based on the flow pattern map discussed in the previous chapter is given next after briefly discussing the area where the heat transfer coefficient is difficult to measure experimentally.

The condensation heat transfer model assumes here that two types of heat transfer mechanism occur within the tube: convective condensation and film condensation. In the present context the convective flow means axial flow of the condensate along the channel due to the imposed pressure gradient while film condensation refers to the flow of condensate from top of the tube to bottom due to gravity. In most of the earlier models only two flow regimes have been identified; stratified flow and non-stratified flow. But based on the new flow pattern predictions it is important to divide the flow regimes in the five categories: stratified flow, stratified-wavy flow, intermittent flow, annular flow, and mist flow. The heat transfer models according to the prevailing flow regime are often proposed.

4.1 DIFFICULT TEST CONDITIONS

As per condensation heat transfer data the most difficult test conditions to make accurate measurement and prediction are as follows:

4.1.1 Near Flow Regime Transition Zones

If a transition from one phase to another takes place within the quasi-local test section, the mean heat transfer coefficient for the section is an unknown average of the two flow regimes.

4.1.2 Very High and Very Low Vapour Quality

At low vapour quality, the void fraction, ε decreases very rapidly with small changes in vapour quality. At very high vapour quality, void fraction and the liquid film thickness, δ are very sensitive to small changes in the liquid fraction (1-x). It is particularly difficult to accurately measure condensation data at vapour qualities less than 0.05 and above 0.95.

4.1.3 Desuperheating and Subcooling

The condensate formed on the desuperheater before i.e. condensate formed while cooling the vapour to its saturation temperature. This condensate enters the condenser test section and hence the film begins with some initial value of liquid film thickness instead of beginning with zero thickness at vapour quality $x = 1$ and void fraction $\varepsilon = 1$. This effect tends to increase the film thickness, which in turn decreases the heat transfer coefficient measured.

4.1.4 Stable Operating Conditions

All experimental test loops have limited range in which steady state test conditions can be maintained. At low mass velocities, typically a threshold is reached where fluctuation in pressure and flow rate become significant. Pressure fluctuation significantly influences the saturation temperature.

4.1.5 Very Large and Very Small Heat Transfer Coefficient

At high vapour quality and high mass velocity as $(T_{sat} - T_w)$ becomes small it gives large uncertainty in heat transfer coefficient when they are very large. Also when heat transfer coefficients are very small i.e. at low mass velocities, energy balances are less accurate because the change in the cooling water temperature from inlet to outlet in the test-section is small.

4.1.6 Circumferential Variation in Heat Transfer Coefficient

Condensation heat transfer coefficients are reported as mean values around the perimeter of the tube. A sufficient number of thermocouples in the tube wall are required to capture a representative mean wall temperature to determine the mean heat transfer coefficient.

4.2 DEVELOPMENT OF TWO-PHASE HEAT TRANSFER MODEL

The new condensation heat transfer model proposed here assumes three simplified geometries for describing annular flow, stratified-wavy flow and fully stratified flow. In case of annular flow a uniform liquid film thickness is assumed, though the film thickness is not uniform, as at the bottom the liquid gets collected and the thickness at bottom is larger than that at the top, this larger thickness is ignored.

For stratified-wavy flow a stratified angle, θ formed in the tube is taken, this angle is based on the liquid inventory in the tube. This angle θ varies between the maximum value of fully stratified angle θ_{str} at the threshold to fully stratified flow and its minimum value of zero at the threshold to annular flow. In case of intermittent flow and mist flow the flow structure is very complex, for these flow regimes also uniformity in liquid film thickness like that in annular flow, is assumed to make the model simple.

Based on the above two heat transfer mechanisms; convective condensation and film condensation, applied to their respective heat transfer surface areas, the heat transfer coefficient are calculated.

For convective condensation heat transfer coefficient, it is applied to perimeter wetted by the axial flow of liquid film, which refers to the entire perimeter in annular flow, intermittent flow, and mist flows but only part of the perimeter in fully stratified flow and stratified-wavy flows.

The expression for heat transfer coefficient by the axial flow of liquid is given by Thome et al. [5] as

$$\alpha_c = c\,\mathrm{Re}_L^n\,\mathrm{Pr}_L^m\,\frac{k_L}{\delta}\,f_t \tag{4.1}$$

where c, n and m are empirical constants, determined from heat transfer database. The optimal value of exponent on liquid Prandtl number varies from 0.4 to 0.5. The best value for m is found to be 0.5, which is slightly greater than the constant in Dittus-Boelter single phase correlation.

Here the liquid Reynolds number is based on the mean velocity of liquid phase as

$$\mathrm{Re}_L = \frac{4G(1-x)\delta}{(1-\varepsilon)\mu_L} \tag{4.2}$$

Based on their statistical analysis they have given the values of empirical constants, the best value for c and n are found to be c = 0.003 and n = 0.74.

the mean velocity for liquid and vapour phase can be calculated as

$$u_L = \frac{G(1-x)}{\rho_L(1-\varepsilon)} \tag{4.3}$$

$$\text{and } u_V = \frac{Gx}{\rho_V \varepsilon} \tag{4.4}$$

But when the heat transfer database of Thome et al. [5], is compared with the experimental results, it is found that the model is under predicting for intermittent and annular flow regime. In the new model presented here the values of empirical constants are again checked and found that if the value of convective film constant, c is increased by 8 percent i.e. instead of 0.003, it is taken as 0.00324, then the predictions of the new model is very close to the experimental results.

So the expression for heat transfer coefficient for convective film becomes as

$$\alpha_c = 0.00324\,\mathrm{Re}_L^{0.74}\,\mathrm{Pr}_L^{0.5}\,\frac{k_L}{\delta} f_i \tag{4.5}$$

here f_i is the interfacial roughness correction factor.

$$f_i = 1 + \left(\frac{u_V}{u_L}\right)^{1/2} \left(\frac{(\rho_L - \rho_V) g \delta^2}{\sigma}\right)^{1/4} \tag{4.6}$$

The value of interfacial roughness factor f_i tends towards a value of 1 as the film becomes very thin (roughness must be proportional to film thickness) but f_i tends to increase as the slip ratio u_V/u_L increases. Finally f_i tends to decrease as σ increases, since surface tension acts to smooth out the waves. For fully stratified flow, interfacial waves are damped out and hence the above expression becomes

$$f_i = 1 + \left(\frac{u_V}{u_L}\right)^{1/2} \left(\frac{(\rho_L - \rho_V) g \delta^2}{\sigma}\right)^{1/4} \left(\frac{G}{G_{str}}\right) \tag{4.7}$$

when $G < G_{str}$, which produces a smooth variation in the two-phase heat transfer coefficient across this flow pattern transition boundary just like for all the other transition boundaries and the ratio of G/G_{str} acts to damp out the effect of interfacial roughness in stratified flow.

The film condensation heat transfer coefficient for the falling film inside the perimeter of the tube is taken from the Nusselt theory for laminar flow of a falling film. A mean value of heat transfer coefficient for film condensation by Thome et al. [5] is given as

$$\alpha_f = 0.728 \left[\frac{\rho_L (\rho_L - \rho_V) g h_{LV} k_L^3}{\mu_L d (T_{sat} - T_w)}\right]^{1/4} \tag{4.8}$$

In the new model developed here, the effect of void fraction is included in the film heat transfer, as done previously by Jaster and Kosky [18] and Chato [27].

So the expression for film heat transfer coefficient becomes as

$$\alpha_f = 0.728 \varepsilon^{3/4} \left[\frac{\rho_L (\rho_L - \rho_V) g h_{LV} k_L^3}{\mu_L d (T_{sat} - T_w)}\right]^{1/4} \tag{4.9}$$

The heat transfer coefficient for the falling film can also be given with the heat flux q, as

$$\alpha_f = 0.655 \varepsilon^{3/4} \left[\frac{\rho_L (\rho_L - \rho_V) g h_{LV} k_L^3}{\mu_L d q}\right]^{1/3} \tag{4.10}$$

The value of void fraction can be calculated by the logarithmic mean void fraction method discussed earlier. The error in calculating the heat transfer coefficient from both the above equation is negligible.

The condensation heat transfer coefficient for the twp-phase based on these two heat transfer mechanisms can be given as

$$\alpha_{tp} = \frac{\alpha_f (d/2)\theta + (2\pi - 2)(d/2)\alpha_c}{d\pi} \tag{4.11}$$

The stratified angle, θ as mentioned earlier is the upper angle of the tube not wetted by the stratified liquid. The value of the stratified angle θ will be different for different flow regimes prevailing.

For annular flow, intermittent flow and mist flow $\theta = 0$;

For fully stratified flow $\theta = \theta_{str}$;

For stratified-wavy flow θ is obtained by assuming a quadratic interpolation between its maximum value of θ_{str} at G_{str} and its minimum value of zero at G_{wavy} as

$$\theta = \theta_{str}\left[\frac{(G_{wavy} - G)}{(G_{wavy} - G_{str})}\right]^{0.5} \tag{4.12}$$

The values of the mass velocities at stratified flow and stratified-wavy flow at the particular vapour quality are determined from their respective transition equations in the flow pattern map.

Chapter 5

VALIDATION OF THE PROPOSED MODEL

5.1 COMPARISON OF FLOW PATTERN MAPS

The flow pattern map applied here is that of Hajal et al. [4] which is originally presented by Kattan et al. [3] for evaporation and adiabatic flows in small diameter horizontal tubes. Their flow pattern map is a modification of the original Taitel and Dukler [6] flow pattern prediction map.

In the flow pattern map the transition between two flow regimes is presented for a particular condensation condition of mass velocity at a specific temperature. For condensation, when saturation vapour enters a condenser tube then they form a thin liquid film around the perimeter of the tube as an annular flow or they form a liquid layer in the bottom of the tube as a gravity-controlled condensing film around the upper perimeter as the stratified or stratified-wavy flow. As dryout does not occur for condensation so the transition curve labelled G_{wavy} can be supposed to reach its minimum value and then continue on horizontal to the vapour quality of 1.0. This means that a dry and saturated vapour enters the test section (x = 1.0) and undergoes directly into either the annular flow regime or the stratified-wavy flow regime, depending on whether the fixed mass velocity is greater or lesser than the mass velocity at stratified-wavy flow transition. The other boundaries remain the same, assuming the gravity-controlled condensing film around the upper perimeter does not affect them. In a mist flow, it is observed that the layer is from the wall and that a new condensate layer will begin to grow again in its place.

5.1.1 Comparison of Logarithmic Mean Void Fraction Method with other Methods

For evaluation of the void fraction, the use of logarithmic mean void fraction method predicts better the flow pattern transition as compared to Rouhani-Axelsson [24] void fraction method as shown in the Figure 5.1 for R-134a at 40°C and saturation pressure of 1017 kPa in an 8 mm inside diameter tube, setting the mass velocity at 300 kg $m^{-2}s^{-1}$.

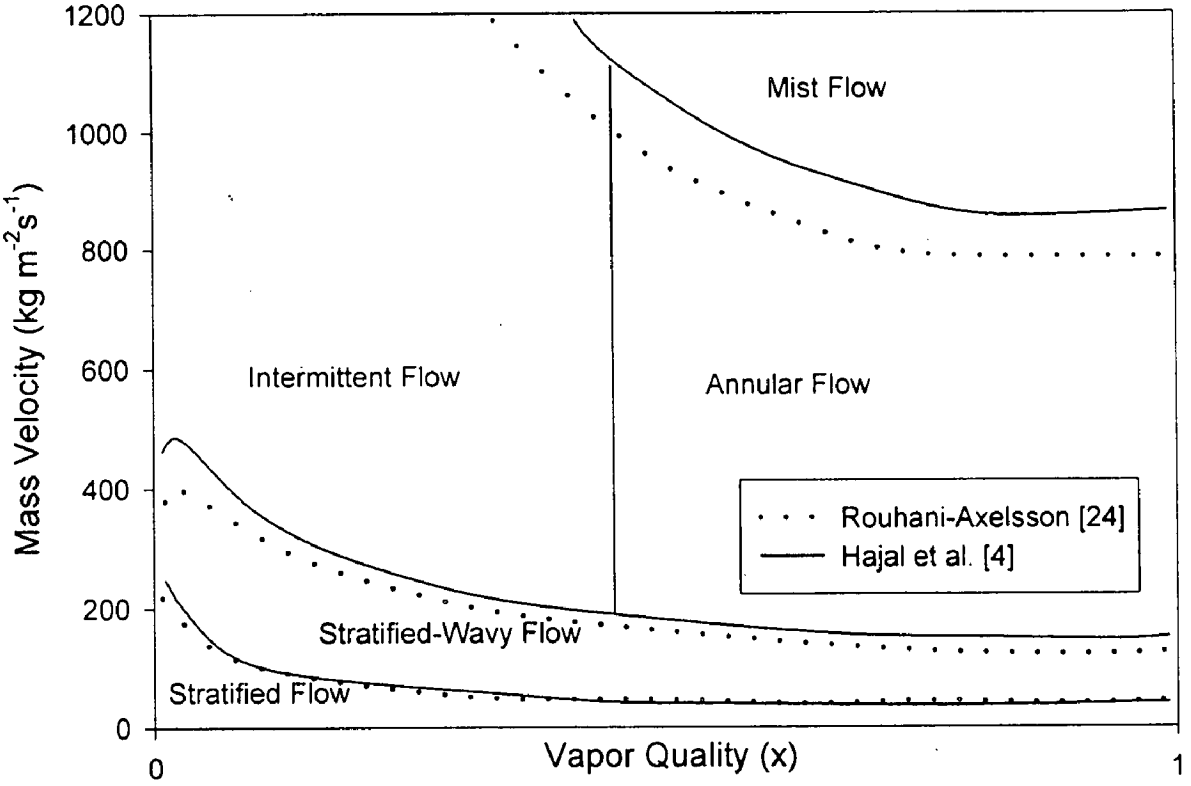

Fig. 5.1 Comparison of flow pattern map for R-134a at 40°C in 8 mm inside diameter tube.

It is observed that there is no effect on the transition between intermittent to annular flow and an extremely minor effect on the stratified to stratified-wavy flow when applying logarithmic mean void fraction method instead of Rouhani-Axelsson [24] void fraction method. The difference between the two mist flow transition curve is more significant but the location of this curve is not critical to the condensation heat transfer model since the annular flow model also predicts the heat transfer coefficient reasonably well for the mist flow.

5.1.2 Comparison with Tandon et al. Flow Map Prediction

Tandon et al. [11] has given flow pattern map prediction method, they divided the flow pattern map in six different flow regimes as wavy flow, plug flow, slug flow, semi-annular flow, and spray flow. The semi-annular flow they have describes is based on two different behaviour of annular flow; one in which the thickness of liquid film is thicker in the bottom than on the top. The spray flow is similar to annular flow where the thickness of liquid film is more uniform.

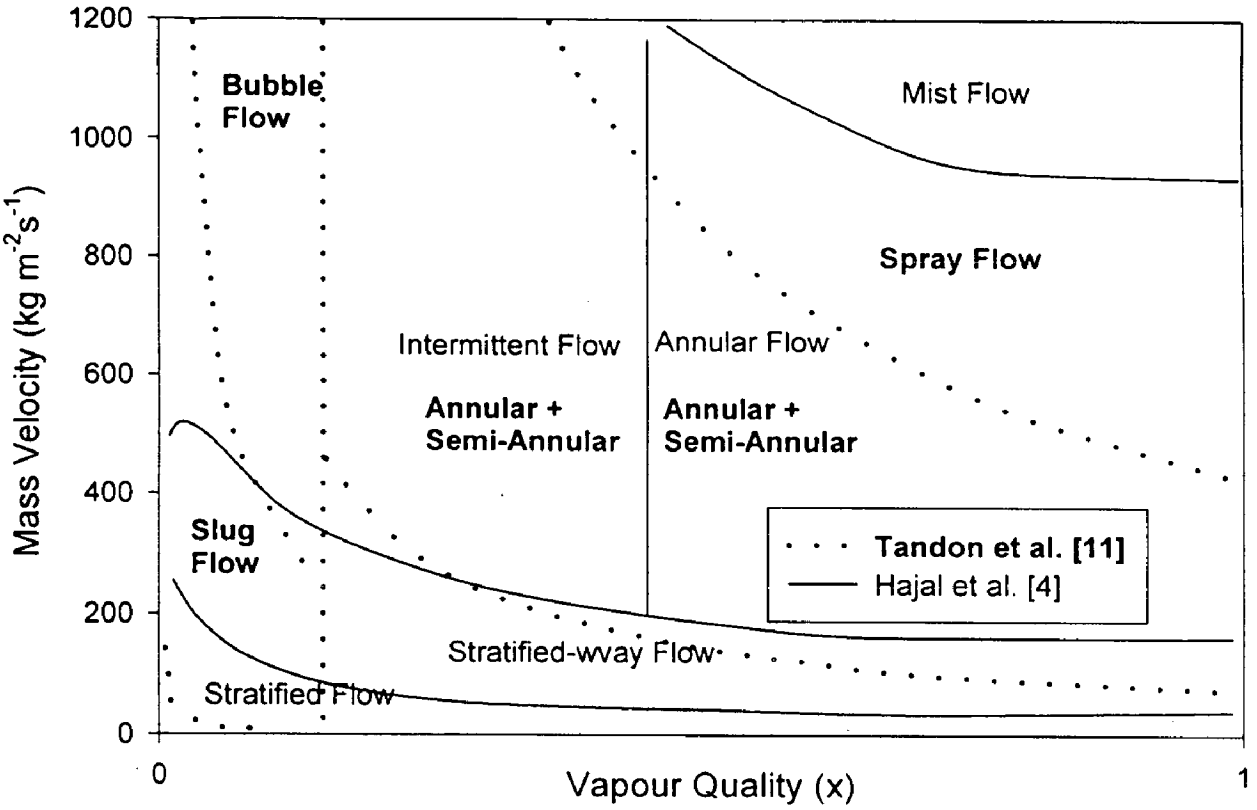

Fig. 5.2 Comparison of flow pattern with the map of Tandon et al. [11] for R-12 at 40°C in 8 mm inside diameter tube.

The flow pattern prediction of Tandon et al. [11] is compared with the present flow pattern prediction for R-12 at 40°C in an 8 mm inside diameter tube setting the fixed mass velocity at 300 kg $m^{-2}s^{-1}$. Their transition curve between wavy flow to semi-annular flow is similar to the transition from stratified flow to stratified-wavy flow, although the discrepancy becomes large at high vapour qualities. Their slug flow regime falls within the intermittent flow regime of present flow pattern map prediction. Their plug flow regime falls within the stratified flow regime of the present map at very low vapour qualities, where there may not be enough vapour to form a continuous vapour phase for a stratified flow. Their semi-annular flow is analogous to intermittent and spray flow is more as annular flow of present flow pattern map prediction.

5.1.3 Comparison with Dobson and Chato and Soliman's Flow Map Prediction

The flow pattern map of Dobson and Chato [16] and that of Soliman [17] is compared with present prediction. Dobson and Chato has given transitions from stable wavy flow to mixed regime of wavy and annular flow and then from this wavy-annular flow to stable annular flow. Dobson and Chato's prediction is based on Soliman's prediction, but increased the transition value of Soliman's modified Froude number from 7 to 20 to better represent their data, which were classified as wavy and annular flows.

Figure shows the comparison of present flow pattern prediction with that of Dobson and Chato and Soliman for R-134a at 35°C in a 7 mm inside diameter tube.

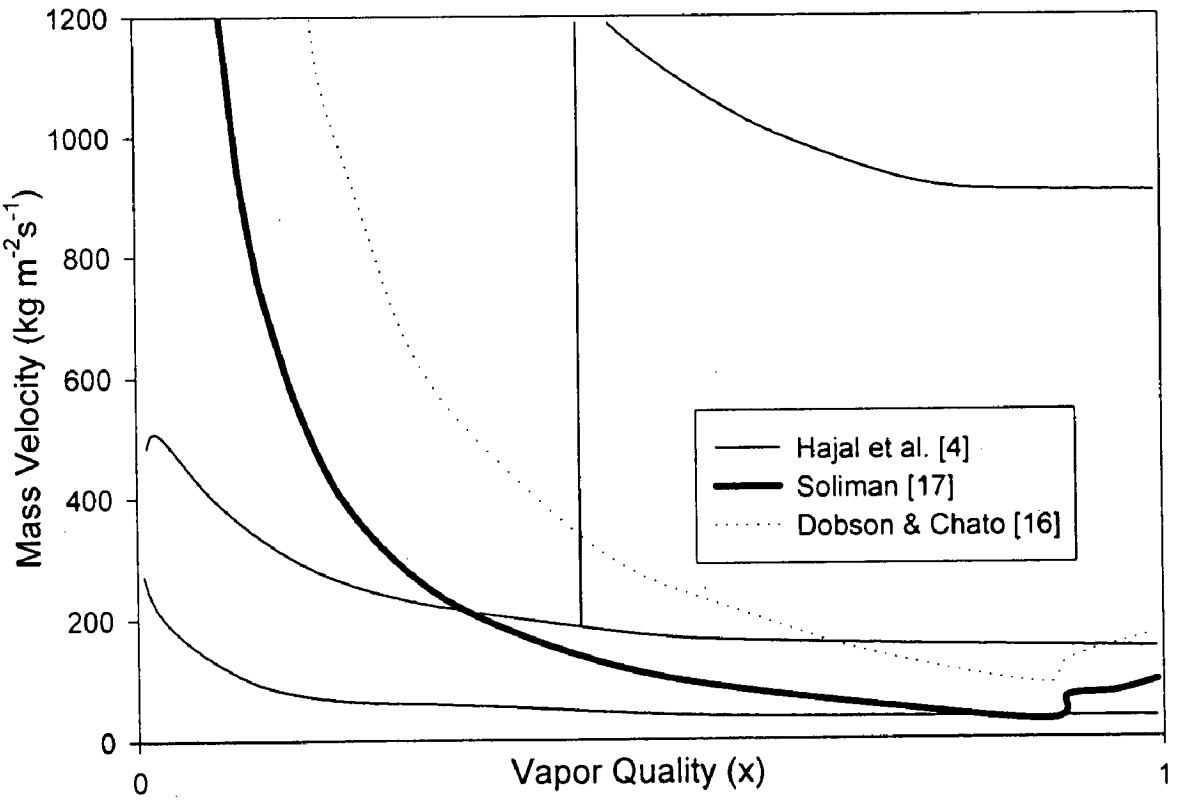

Fig. 5.3 Comparison of flow pattern with the map of Dobson and Chato [16] and Soliman [17] transition for R134 at 35°C.

5.1.4 Comparison with Flow Pattern Map Prediction of Cavallini et al.

The flow pattern map predicted by Cavallini et al. [21] for R-12 at 40°C in an 8 mm inside diameter tube is compared with present flow pattern map prediction. In their map

they classified the flow regimes as annular flow, stratified-wavy flow and slug flow. As it can be observed from the graph that their annular flow region coincides with annular flow regime of present map and their slug flow region for the most part correctly falls within the intermittent flow regime. Their stratified-wavy flow region is not well defined and this may refer to the intermittent and stratified-wavy flow of present flow pattern map prediction method. Cavallini et al. [21] have neglected the fully stratified flow regime which is predicted well in the present flow pattern map prediction.

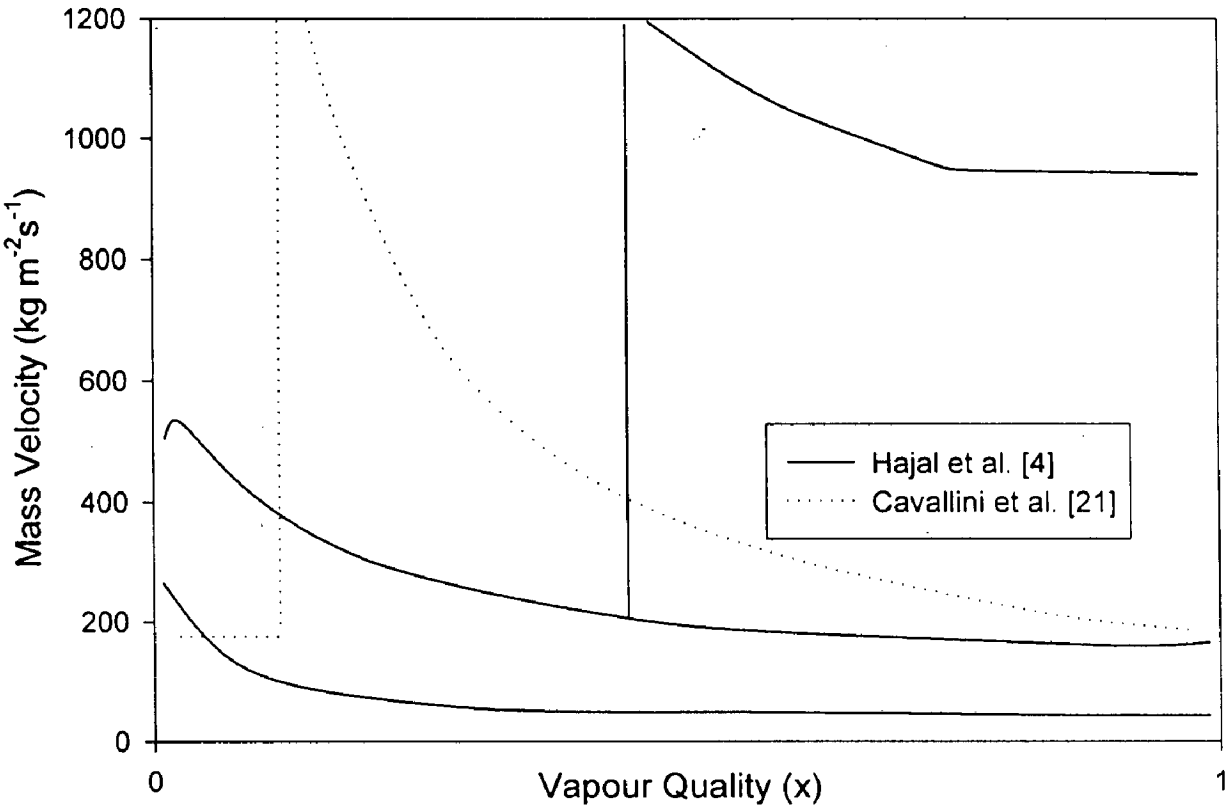

Fig. 5.4 Comparison of flow pattern with the map of Cavallini et al. [21] for R-12 at 40°C.

In summary, the subjective nature of classifying flow pattern observations from one observer to another, the difference in opinion on flow pattern definitions, and even disagreement about which classification to use, means that a quantitative comparison between competing methods is not always realistic. Even so, numerous similarities and overlaps between flow regime zones and flow transition boundaries are found in the above comparisons. Based on the above observations it is justifiable to apply the present

Hajal et al. [4] method for condensation flow pattern map based on the logarithmic mean void fraction method.

5.2 COMPARISON OF THE PROPOSED MODEL WITH EXISTING MODELS

The heat transfer coefficients for different refrigerant and hydrocarbons at some certain condition, obtained from the present computerised model is compared with the experimental results at the same mass velocity and same physical conditions. These results of computerised model are also compared with some of the existing models. To compare the new presented computerised model with the other models and experimental results, graph for heat transfer coefficient as a function of vapour quality is plotted. Some of the compared results for the refrigerants like R-11, R-12, R-22, and R-134a etc are shown here under.

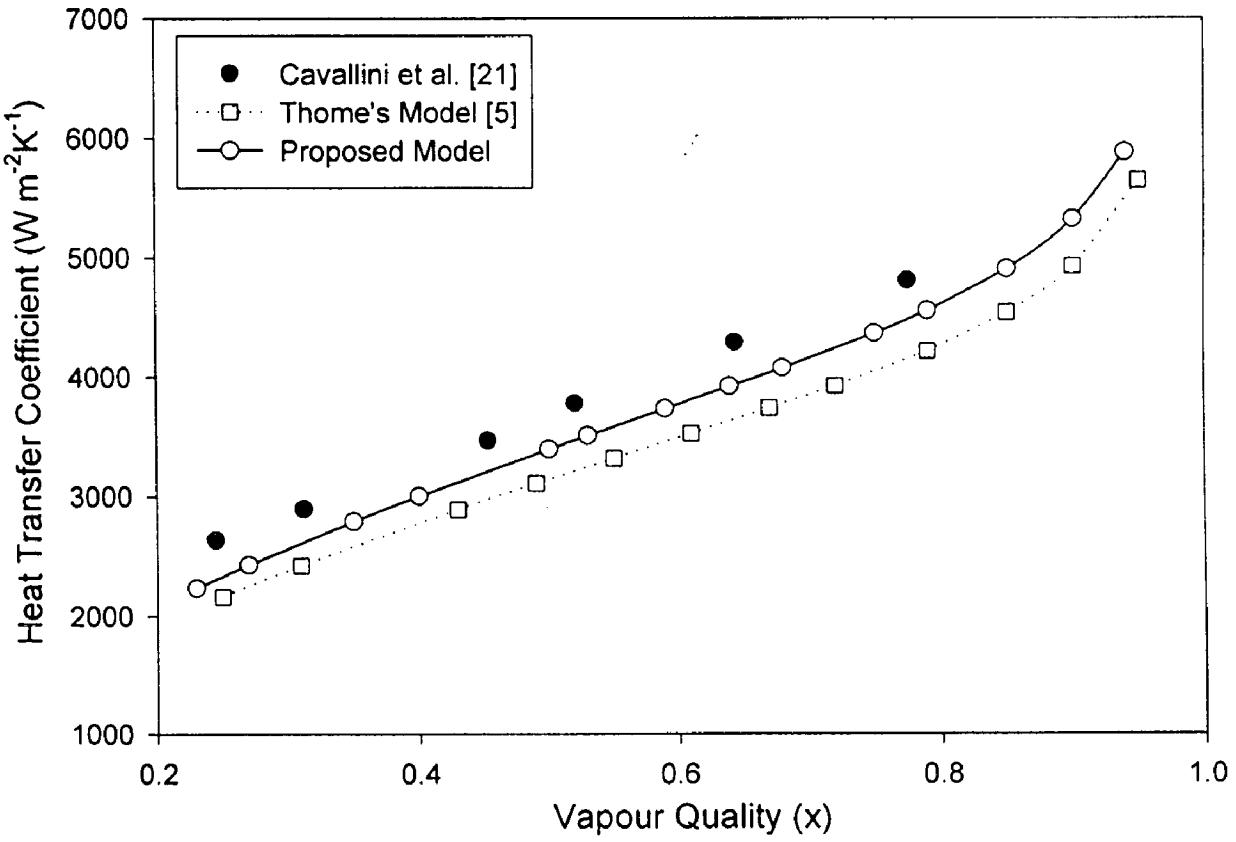

Fig. 5.5 Comparison of heat transfer coefficient with Cavallini et al. experiment results for R-134a at G = 400 kg $m^{-2}s^{-1}$ and T_s = 40°C.

Fig. 5.5 shows the comparison of heat transfer coefficient calculated by the present model with the model of Thome et al. [5] and also with the experimental results of Cavallini et al. [21] for R-134a at mass velocity of 400 kg $m^{-2}s^{-1}$, saturation temperature of 40°C in a

tube of 8 mm inside diameter. It is observed by the graph that the proposed model is predicting better and much closer to the experimental results. The proposed model under predicts the experimental data by 14 percent. However, widely accepted Thome's model under predicts the experimental data by 20 percent.

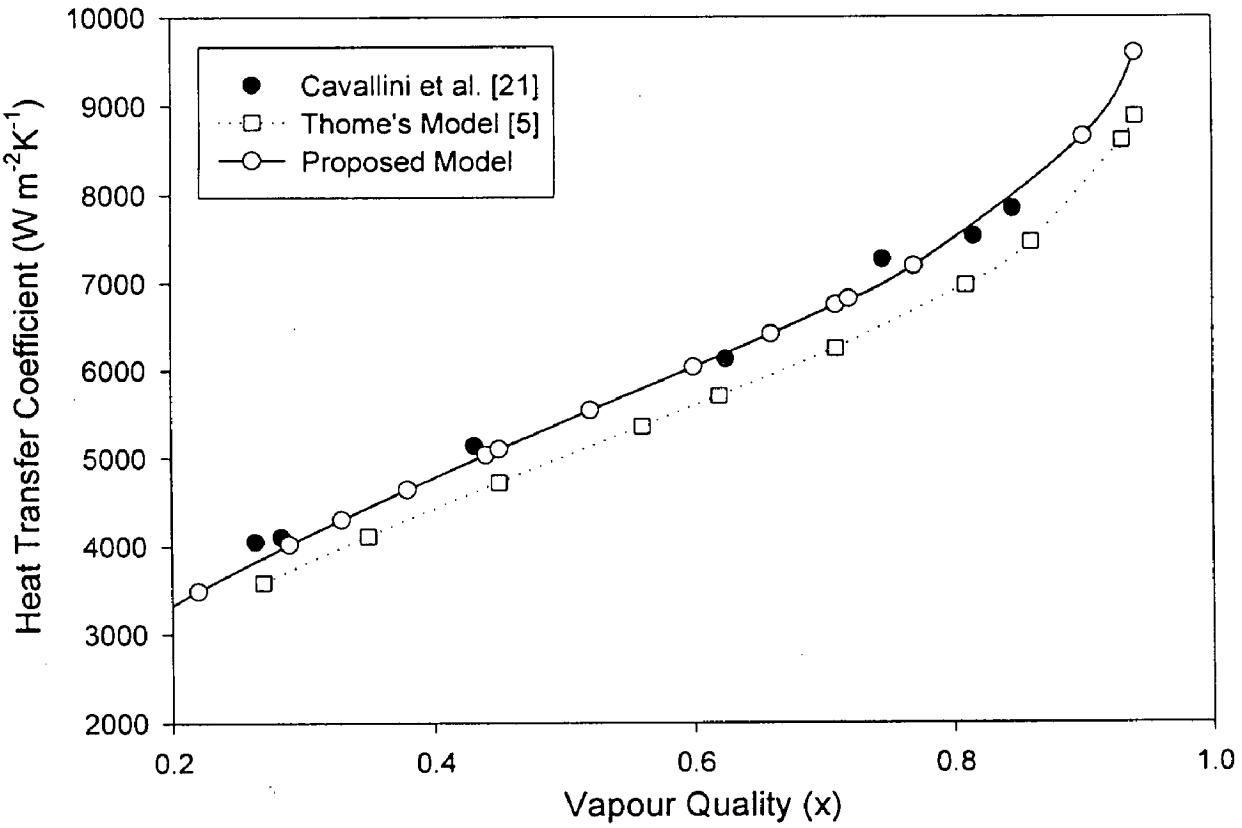

Fig. 5.6 Comparison of heat transfer coefficient for R-22 at G = 750 kg $m^{-2}s^{-1}$ and T_s = 40°C.

Fig. 5.6 shows the comparison of heat transfer coefficient calculated by the present model with the model of Thome et al. [5] and also with the experimental results of Cavallini et al. [21] for R-22 at mass velocity of 750 kg $m^{-2}s^{-1}$, saturation temperature of 40°C in a tube of 8 mm inside diameter. It is observed by the graph that the proposed model is predicting better and much closer to the experimental results. The proposed model predicts heat transfer coefficient with an error of 3 percent while the Thome's model under predicts the experimental data by 10 percent.

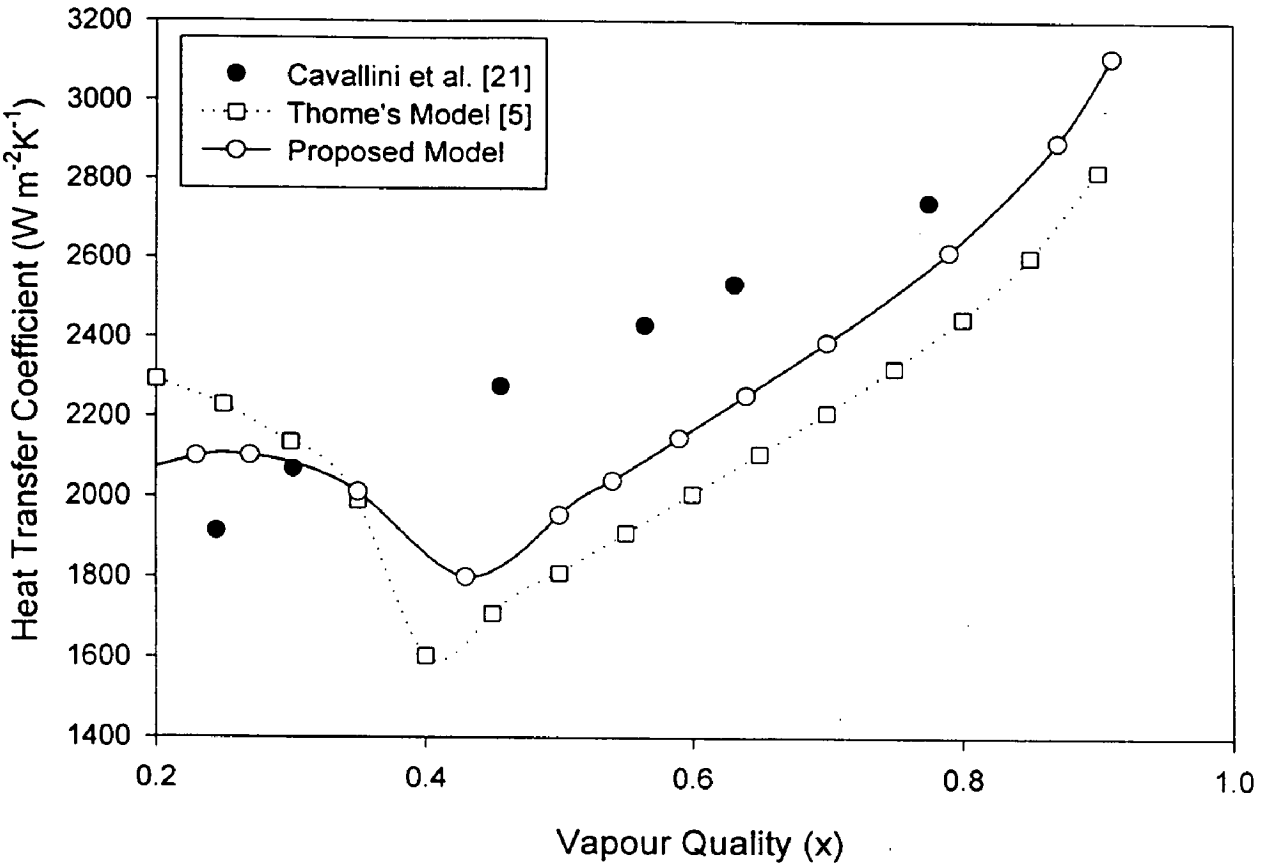

Fig. 5.7 Comparison of heat transfer coefficient for R-134a at G = 200 kg $m^{-2}s^{-1}$ and T_s = 40°C.

In Fig. 5.7 the comparison of heat transfer coefficient obtained by present model is compared with original model of Thome et al. [5] and also with the experimental data of Cavallini et al. [21]. Although the proposed model is predicting better for R-134a at mass velocity of 200 kg $m^{-2}s^{-1}$ and saturation temperature of 40°C in a tube of 8 mm inside diameter, but it is observed that at the transition the heat transfer coefficient falls rapidly and then again rise rapidly at vapour qualities near 0.4. The proposed model under predicts the experimental data by 14.5 percent while the Thome's model under predicts the experimental data by 23 percent.

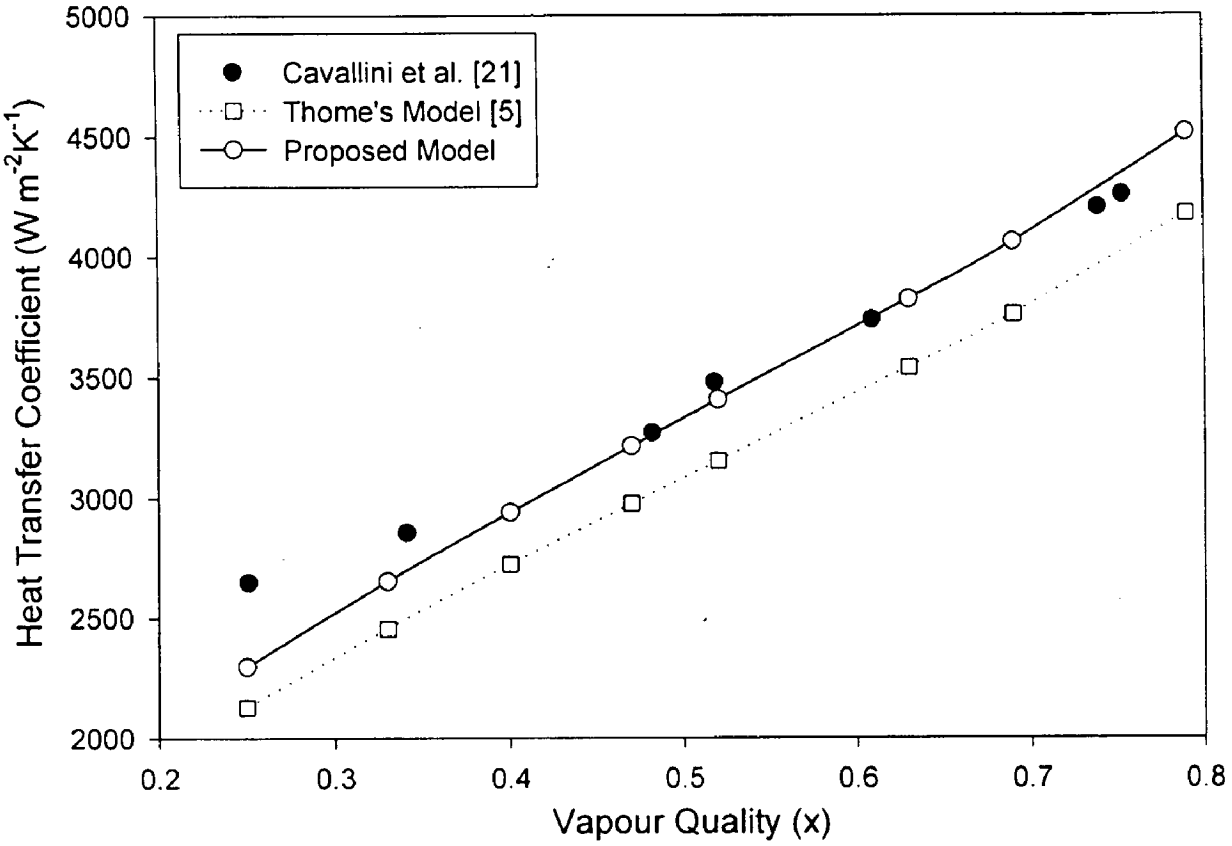

Fig. 5.8 Comparison of heat transfer coefficient for R-22 at G = 400 kg $m^{-2}s^{-1}$ and T_s = 40°C.

Fig. 5.8 shows the comparison of heat transfer coefficient calculated by the present model with the original model of Thome et al. [5] and also with the experimental results of Cavallini et al. [21] for R-22 at mass velocity of 400 kg $m^{-2}s^{-1}$, saturation temperature of 40°C in a tube of 8 mm inside diameter. It is observed by the graph that the proposed model is predicting better and much closer to the experimental results. The proposed model predicts heat transfer coefficient with an error of 4 percent while the Thome's model under predicts the experimental data by 12 percent.

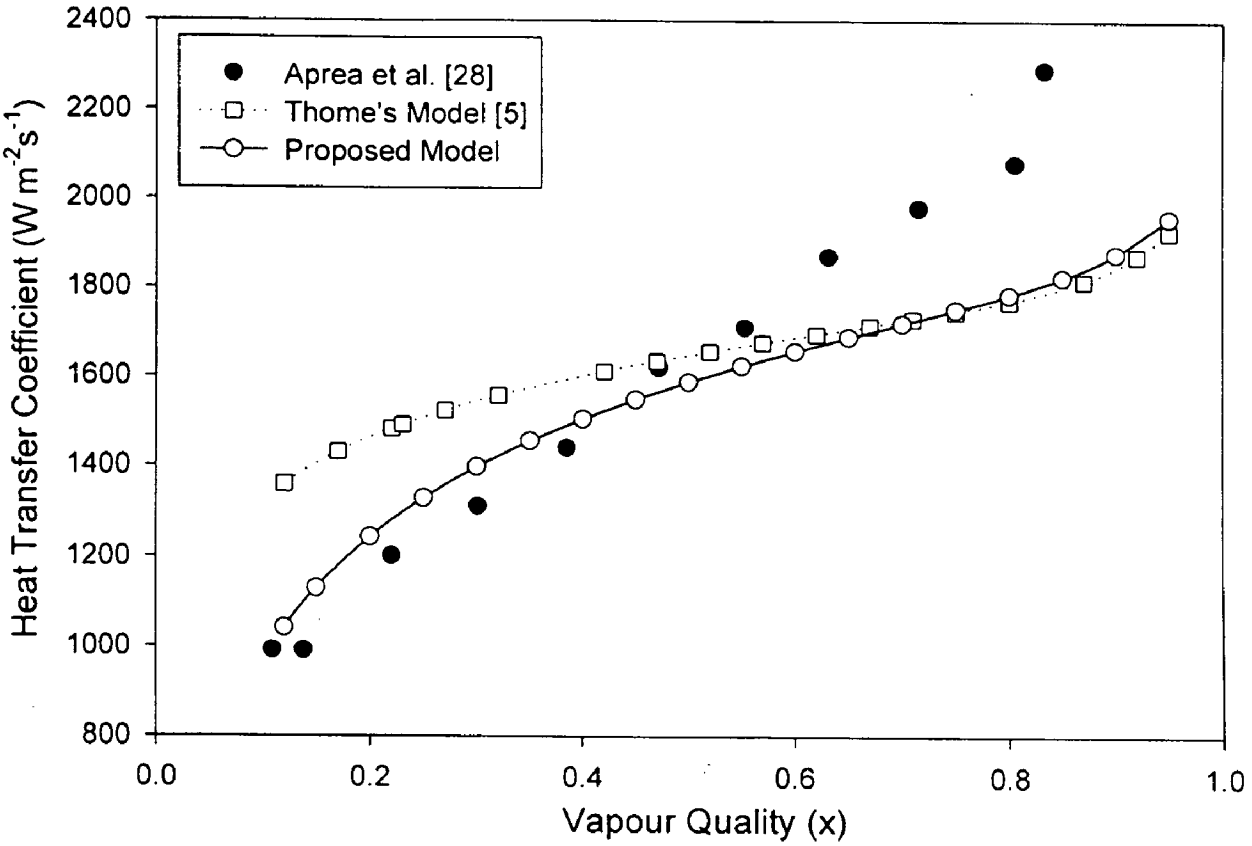

Fig. 5.9 Comparison of heat transfer coefficient for R-22 at G = 120 kg $m^{-2}s^{-1}$ and T_s = 39.6°C.

In Fig. 5.9 the comparison of heat transfer coefficient calculated by the proposed model with the original model and also with the experimental results of Aprea et al. [28] is given. In this graph heat transfer coefficient is calculated for R-22 at mass velocity 120 kg $m^{-2}s^{-1}$ and saturation temperature 39.6°C and a tube of inside diameter of 20 mm is taken. The proposed model is predicting the heat transfer coefficient close to the experimental values at low vapour quality. At higher vapour quality ($x > 0.6$) the prediction by the proposed model and the Thome's model are very close to each other. But the deviation from experimental values is very high. The proposed model predicts heat transfer coefficient with an error of 11 percent while the Thome's model predicts the heat transfer coefficient with an error of 18 percent.

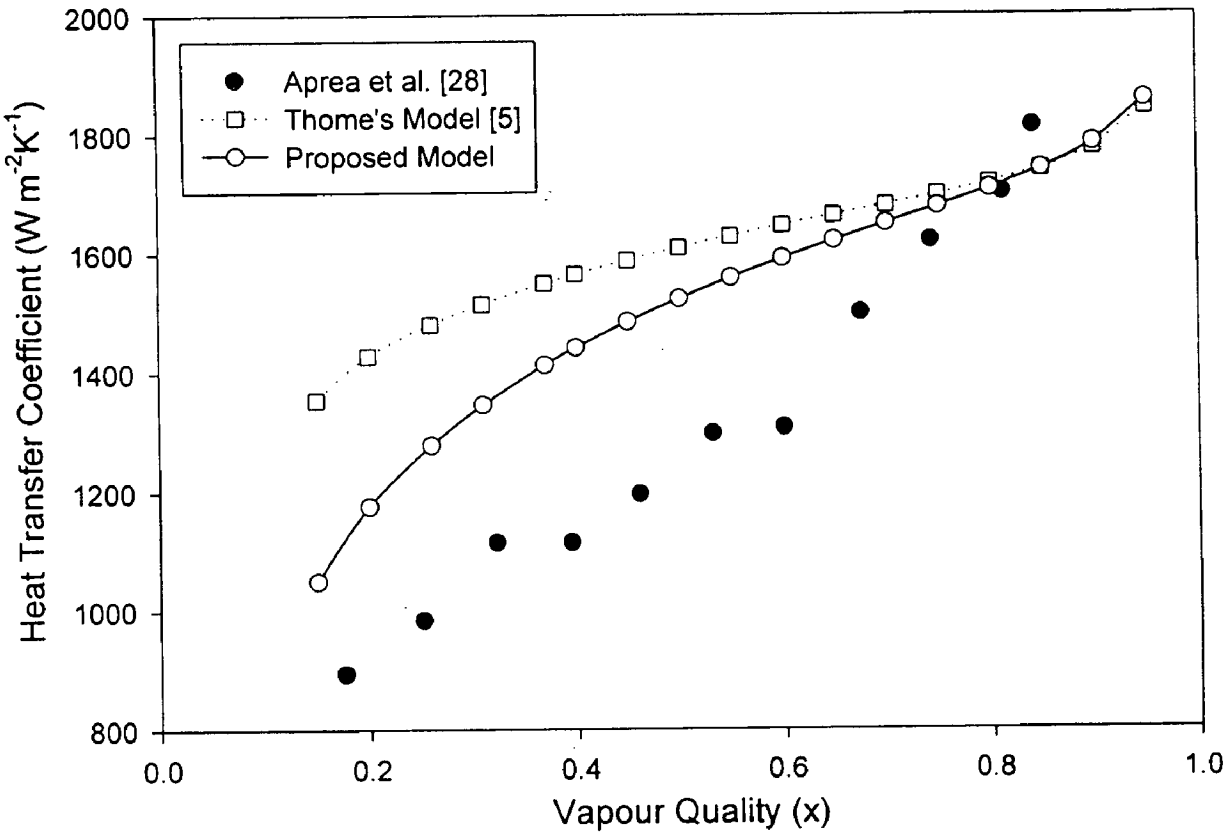

Fig. 5.10 Comparison of heat transfer coefficient for R-22 at G = 90 kg $m^{-2}s^{-1}$ and T_s = 39.6°C.

In Fig. 5.10 the comparison of heat transfer coefficient calculated by the proposed model with the original model and also with the experimental results of Aprea et al. [28] is given. In this graph heat transfer coefficient is calculated for R-22 at mass velocity 90 kg $m^{-2}s^{-1}$ and saturation temperature 39.6°C and a tube of larger inside diameter of 20 mm is taken. The proposed model is predicting better especially at low vapour qualities but at higher vapour qualities the prediction by the proposed model and the Thomes's model are very close to each other. But the deviation from the experimental values is high. The proposed model over predicts heat transfer coefficient with by 17 percent while the Thome's model over predicts the experimental data by 29 percent.

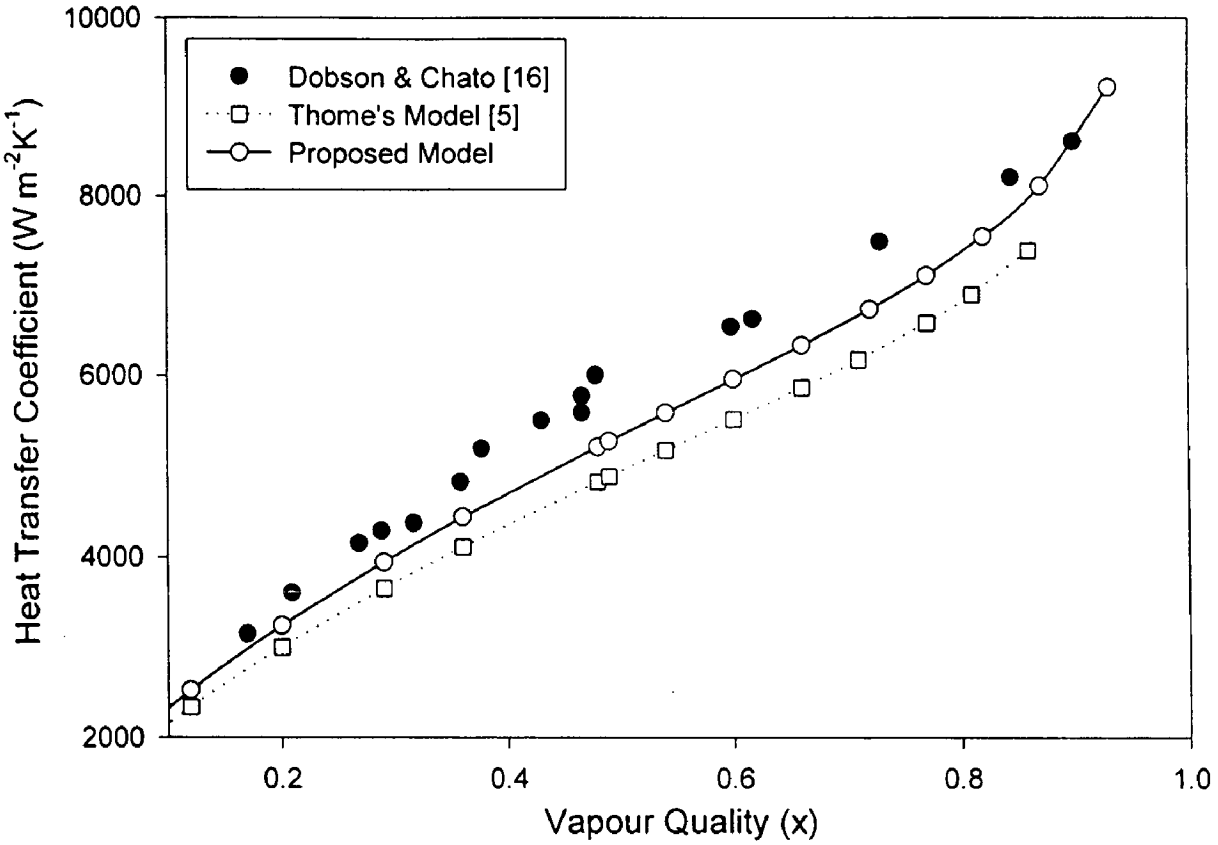

Fig. 5.11 Comparison of heat transfer coefficient for R-22 at G = 650 kg $m^{-2}s^{-1}$ and T_s = 35°C.

Fig. 5.11 shows the comparison of heat transfer coefficient calculated by the proposed computerised model with the original model of Thome et al. [5] and also with the experimental results of Dobson and Chato [16] for R-22 at mass velocity 650 kg $m^{-2}s^{-1}$ and the saturation temperature of 35°C for a tube of inside diameter 7.04 mm. It is observed here that the proposed model is better predicting as compared to the Thome's model. The proposed model under predicts heat transfer coefficient with 4.5 percent while the Thome's model under predicts the experimental data by 9.5 percent.

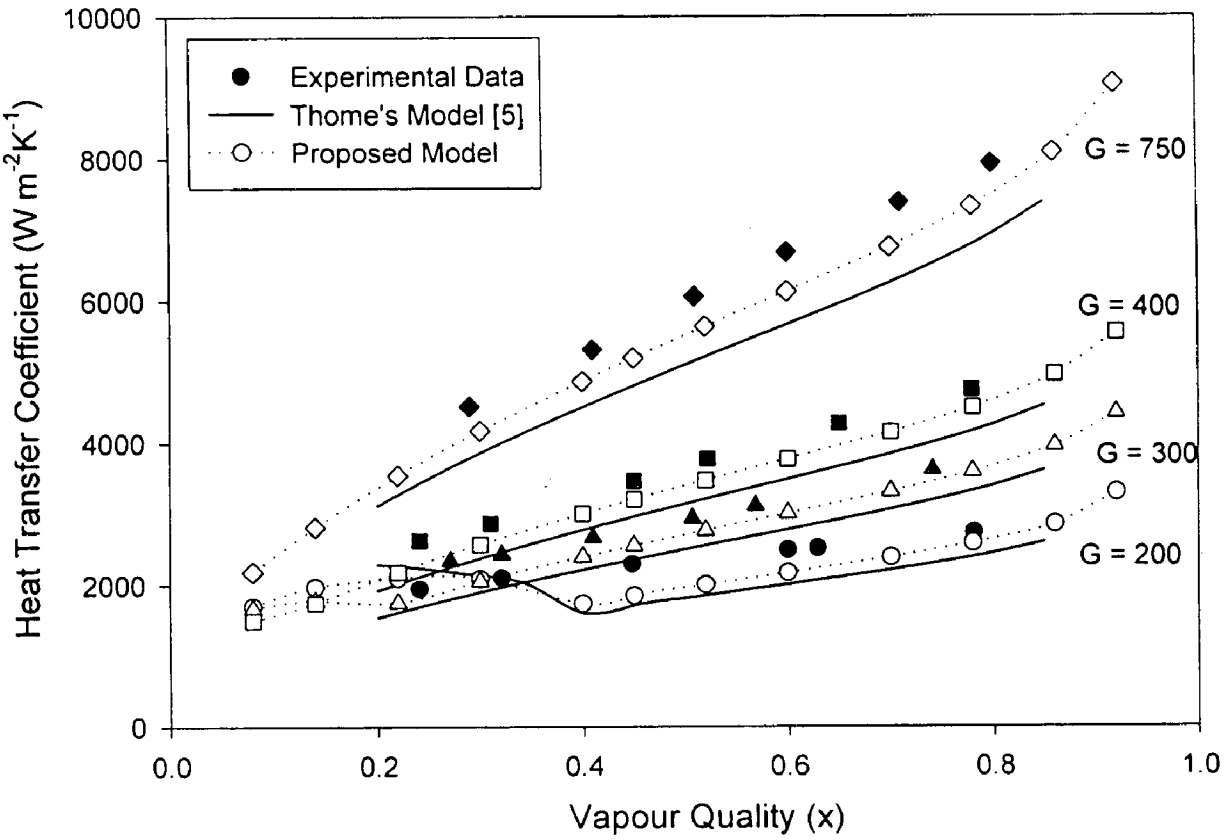

Fig. 5.12 Comparison of heat transfer coefficient for R-134a at 40°C for different mass velocities.

Fig. 5.12 presents the comparison of heat transfer coefficient R-134a for different mass velocities at saturation temperature of 40°C in 8 mm inside diameter tube. The heat transfer coefficient obtained by proposed model is compared with the original model and also with experimental heat transfer database.

To compare the heat transfer coefficient with the experimental results, the data taken are from various sources like those of Cavallini et al. [12, 21], Tandon et al.[11], Shah [15] and Dobson and Chato's [16]. The heat transfer coefficient plotted as a function of vapour quality, falls monotonically from large values at high vapour qualities, as the film thickness is very thin there, to small values at low vapour qualities. Hence the slope of the data curves increase with increasing mass velocity.

For high vapour qualities all these data falls within the annular or intermittent flow regime and at the lowest vapour qualities and mass velocities they reach the stratified-

wavy flow and fully stratified flow regimes. The effect of inclusion of interfacial roughness factor is checked by taking heat transfer data with and without interfacial roughness factor. It is noted that the, inclusion of the interfacial roughness factor significantly improves the accuracy.

5.3 PARAMETRIC STUDY OF THE MODEL

Fig. 5.13 provides a statistical view of the accuracy of the new computerised model. However, in order to be useful as a method for the optimisation of heat exchangers, it is important that the method respect the characteristic trends in the data i.e. the effect of individual variables on the prediction of the local heat transfer coefficient. In the figure, the values above the diagonal represents over prediction and the values below the diagonal presents the under predicted data.

The effects of various parameters and the variables on the local heat transfer coefficient are studied. On studying the heat transfer coefficient curves as a function of vapour quality, it is observed that the model is correctly capturing the slope of the heat transfer coefficient vs. vapour quality as mass velocity changes. The scatter is larger at high and very low vapour qualities, where measurements typically have larger errors or may include desuperheating or subcooling effects. The data at very high void fraction tends to be most difficult to predict because a very small changes of 0.005 in void fraction has a notable effect on the film thickness when the void fraction is larger than 0.95. The effect of film thickness on heat transfer coefficient is studied, it is observed that at very high vapour qualities the film thickness is very small, it is affected by any pre existing condensate formed during desuperheating, which causes the model to over predict the heat transfer coefficient. The lowest pressure represented in the database is 78 kPa while the highest is 3184 kPa. The new model works just as well at low reduced pressure as at high ones, which is from 0.02 to 0.8, while previous prediction methods are not reliable over such a wide range.

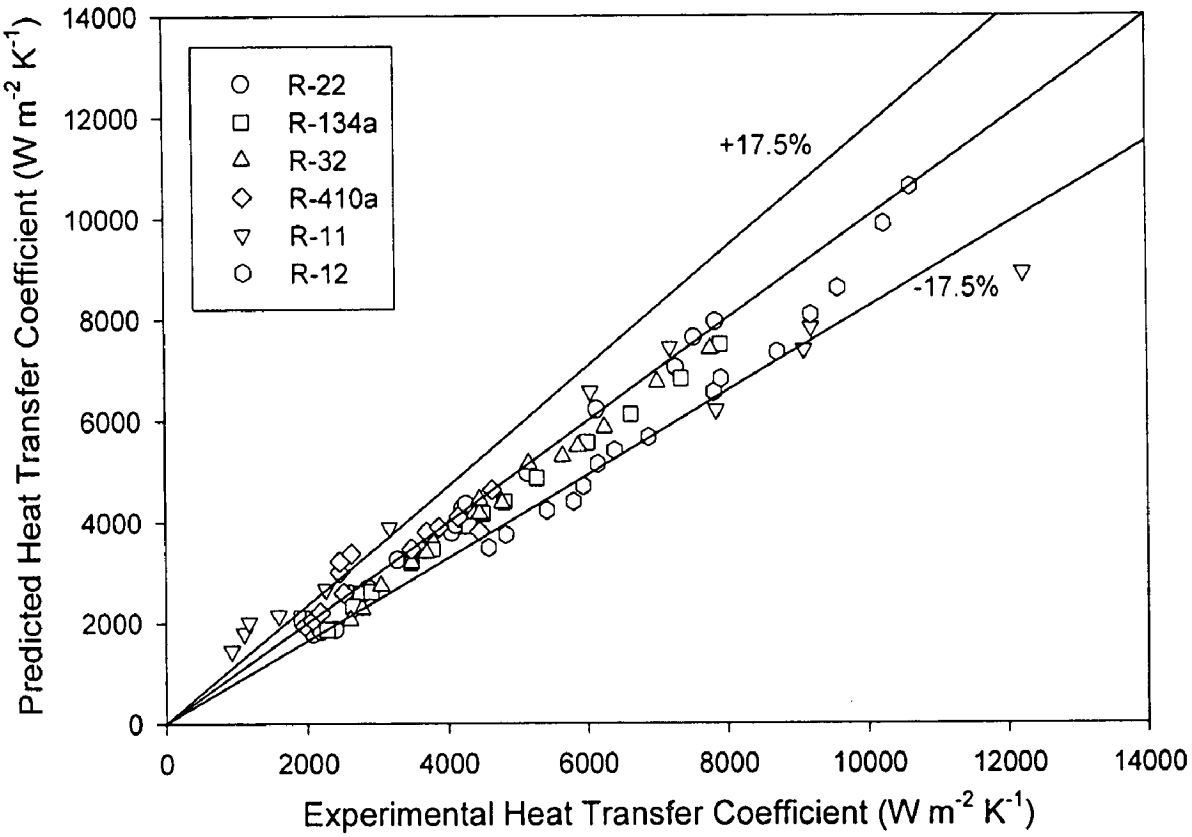

Fig. 5.13 Comparison of heat transfer coefficient predicted by the proposed model with experimental values.

The range in mass velocities here is very large, 24 to 1022 kg $m^{-2}s^{-1}$, and the new model predicts the entire range with good accuracy. The band of errors is somewhat larger at low mass velocities since these flows are in the stratified-wavy and fully stratified regimes, or in annular or intermittent flow near the transition, where the prediction of the heat transfer coefficient is sensitive to the calculation of the dry angle and the G_{wavy} flow pattern transition, respectively. The range of internal diameter represented is very broad, i.e. from 3.1 to 21.4 mm, which covers nearly all the sizes of the heat transfer tubes used in the industrial practice. The predictions for most of the tube sizes are pretty well, with a good accuracy.

The prediction works equally well for all the flow regimes. The stratified flow regime is the only one which is scattered from the experimental results, these data are difficult to measure and predict as, it is difficult to maintain steady-state conditions and get good energy balances at these very low mass velocities and also the variation in the falling film

heat transfer coefficient around the perimeter of the tube may not be captured correctly. Also it is observed that applying the annular flow heat transfer structure to intermittent flow just works as well as for annular flow itself. For mist flow, applying the annular flow heat transfer structure ($\theta = 0$) gives a good prediction.

CONCLUSIONS AND RECOMMENDATIONS

The heat transfer model developed here based on the flow pattern is studied. The change in heat transfer coefficient with change in various parameters viz. vapour quality, mass velocity, tube diameter is studied. By the observation of the predictions of the proposed model and the predictions of the Thome's model, the conclusions are listed here under.

6.1 CONCLUSIONS

The present flow regime based transfer model is compared with the model of Thome at al. [5] then it is also compared with the experimental results and some of the other models.

Based on the comparison of the proposed model with other existing models and experimental results, the conclusions are:

(1) The proposed heat transfer model for condensation inside smooth horizontal tube has been developed for different refrigerants like R-11, R-12, R-22, R-32, R-113, R-125, R-134a, R-404A, R-410A, and some of the hydrocarbons like propane, n-butane, iso-butane and propylene.

(2) The proposed model is valid for a large range of parameters and physical conditions like mass velocities from 24 to 1022 kg $m^{-2}s^{-1}$, vapour qualities from 0.03 to 0.97, reduced pressures from 0.02 to 0.8 and tube internal diameters from 3.1 to 21.4 mm.

(3) The Thome's model [5] has predicted the heat transfer coefficient within an error band of ± 20 percent whereas, the proposed model is predicting the heat transfer coefficient within an error band of ± 17.5 percent for 80 percent of the data points taken, which is a good improvement from the Thome's model [5].

6.2 RECOMMENDATIONS FOR FUTURE WORK

For condensation inside smooth horizontal tubes a number of heat transfer models are available, some of them are based on flow pattern. But the fact remains that most of them

are suitable for a limited application. They don't have a wide range of parameters i.e. mass velocity, reduced pressure, tube diameter etc. Further, experimental data are not available for condensation of many halogenated refrigerants near the critical temperature to possibly extend the confidence on available models. It is also observed that a model suitable for a particular refrigerant doesn't predict well for other refrigerant. Most of the models have not considered all the flow regimes and no models is generalised and covers the entire map of two phase flow regimes.

Future work is certainly needed so as:

(1) To extend the validity range of existing correlations and/or to develop new models which can predict for a larger range viz. mass velocity, reduced pressure, tube diameter etc.

(2) Highly accurate experimental results are required for better validation of the model especially at the difficult test conditions.

(3) Pure analytical model may be developed for condensation inside the smooth horizontal tube, using five flow regime transition lines for various refrigerant mass velocities, tube shape and tube diameters, using computational intelligence.

REFERENCES

1. Kattan N., Thome J. R., and Favrat D., "Flow boiling in Horizontal Tubes: Part 1 – Development of a Diabatic Two-Phase Flow Pattern Map," Journal of Heat Transfer, vol. 120, pp. 140-147, 1998.
2. Kattan N., Thome J. R., and Favrat D., "Flow boiling in Horizontal Tubes: Part 2 – New Heat Transfer Data for Five Refrigerants," Journal of Heat Transfer, vol. 120, pp. 148-155, 1998.
3. Kattan N., Thome J. R., and Favrat D., "Flow boiling in Horizontal Tubes: Part 3 – Development of a new Heat Transfer model based on Flow Pattern," Journal of Heat Transfer, vol. 120, pp. 156-165, 1998.
4. Hajal J. El., Thome J. R., and Cavallini A., "Condensation in Horizontal tubes, Part 1: Two-Phase Flow Pattern Map," International Journal of Heat and Mass Transfer, vol. 46, pp. 3349-3363, 2003.
5. Thome J. R., Hajal J. El., Cavallini A., "Condensation in Horizontal tubes, Part 2: New Heat Transfer Model Based on Flow Regimes," International Journal of Heat and Mass Transfer, vol. 46, pp. 3365-3387, 2003.
6. Taitel Y. and Dukler A. E., "A model for predicting flow regime transitions in horizontal and near horizontal gas-liquid flow," A I ChE J., vol. 22(2), pp. 43-55, 1976.
7. Baker O., "Design of pipelines for simultaneous flow of oil and gas," Oil Gas Journal, vol. 53, pp. 185-195, 1953.
8. Hashizume K., "Flow pattern and void fraction of refrigerant two-phase flow in a horizontal pipe," JSME, vol. 26(219), pp. 1597-1602, 1983.
9. Mandhane J. M., Gregory G. A., and Aziz K., "A flow pattern map for gas liquid flow in horizontal pipes," International Journal of Multiphase flow, vol. 1, pp. 537-553, 1974.
10. Breber G., Palen J.W., Taborek J., "Prediction of horizontal tube-side condensation of pure components using flow regime criteria," Journal of Heat Transfer, vol. 102, pp. 471-476, 1980.

11. Tandon T. N., Varma H. K., and Gupta C. P., "A new flow regime map for condensation inside horizontal tubes," ASME Journal of Heat Transfer, vol. 104 pp. 763–768, 1982.
12. Cavallini A. et al., "Intube condensation of halogenated refrigerants," ASHARE Trans., vol. 108 (1), pp. 4507, 2002.
13. Ackers W. W., and Rosson H. F., "Condensation inside a horizontal tube," Chemical Engineering Progress Symposium Ser, vol. 56, pp. 145-149, 1960.
14. Sardesai R. G., Owen R. G., and Pulling D. J., "Flow regimes for condensation of a vapour inside a horizontal tube," Chemical Engineering Science, vol. 36, pp. 1173–1180, 1981.
15. Shah M. M., "A general correlation for heat transfer during film condensation inside pipes," International Journal of Heat and Mass Transfer, vol. 22, pp. 547–556, 1979.
16. Dobson M. K., and Chato J. C., "Condensation in smooth horizontal tubes," ASME Journal of Heat Transfer, vol. 120, pp. 193–213, 1998.
17. Soliman H. M., "On the annular-to-wavy flow pattern transition during condensation inside horizontal tubes," The Canadian Journal of Chemical Engineering, vol. 60, pp. 475–481, 1982.
18. Jaster H. and Kosky P. G., "Condensation heat transfer in a mixed flow regime," Int J Heat Mass Transfer, vol. 19, pp. 95–99, 1976.
19. Sarma P. K. et al., "Convective condensation heat transfer in a horizontal condenser tube," International Journal of Thermal Science, vol. 41, pp. 295-301, 2002.
20. Boissieux X. et al., "Two-phase heat transfer coefficient of three HFC refrigerants inside a horizontal smooth tube, part-II: condensation," International Journal of Refrigeration, vol. 23, pp. 345-352, 2000.
21. Cavallini et al., "Experimental investigation on condensation heat transfer and pressure drop of new HFC refrigerants (R-134a, R-125, R-32, R-410A, R-236ea) in a horizontal tube," International Journal of Refrigeration, vol. 24, pp. 73–87, 2001.
22. Nusselt W., "Die Oberflachenkondensation des Wasserdampfes," Z Ver Dt Ing, vol. 60, pp.541-546, 569-575, 1916.
23. Kosky P. G. and Staub F. W., "Local condensing heat transfer coefficient in the annular flow regime," AIChE, vol. 17, pp. 1037-1043, 1971.

24. Rouhani Z. and Axelsson E., "Calculation of void volume fraction in the subcooled and quality boiling regions," International Journal of Heat and Mass Transfer, vol. 13, pp. 383-393, 1970.
25. Biberg D., "An explicit approximation for the wetted angle in two-phase stratified pipe flow," Canadian Journal of Chemical Engineering, vol. 77, pp. 1221-1224, 1999.
26. Zurcher O., Thome J. R., and Favrat D., "Evaporation of ammonia in a smooth horizontal tube: heat transfer measurement and predictions," Journal of Heat Transfer, vol. 121, pp.89-101, 1999.
27. Chato J. C., "Laminar condensation inside horizontal and inclined tubes," ASHARE Journals, vol. 4, pp. 52-60, 1962.
28. Aprea C., Greco A. and Vanoli G. P., "Condensation heat transfer coefficient for R-22 and R-407C in gravity driven flow regime within a smooth horizontal tube," International Journal of Refrigeration, vol. 26, pp. 393-401, 2003.
29. Cavallini A. et al., "Condensation inside and outside smooth and enhanced tubes- a review of recent research," International Journal of Refrigeration, vol. 26, pp. 373-392, 2003.
30. Rohsenow W. M., "Development in heat transfer," Edward Arnold (Publishers) Ltd., 1964.

Annexure A

/* PROGRAMME FOR CALCULATION OF TWO-PHASE HEAT TRANSFER COEFFICIENT*/

```
#include <iostream.h>
#include <math.h>
#include <ctype.h>
#include <conio.h>
#include <fstream.h>
enum flowtype {annular, intermittent, mist, stratified_wavy, stratified};
int main()
{
float G,x,d;
float rhol,rhov,sigma, g=9.81, mul, muv,cpl,kl,hlv,Tsw;
float epsh,epsra,eps;
float Al,Av,Ald,Avd,theta_str,A,hld,pid;
float Gwavy,Gmist,xia, Gbubly,Gstr,zeta;
float wfno,const1=226.3*226.3;
float del,Rel,ul,uv,fi,prndl,h_c,h_f,theta,htp;
ofstream out("Are.txt");
flowtype flow;
/* The input data i.e. tube diameter'd', mass velocity 'G' and physical properties*/
d=0.0107;
G=100;
```

```
rhol=1167;
rhov=43;
mul=1.79e-4;
muv=1.2e-5;
cpl=867;
kl=0.08;
sigma=.00682;
hlv=389994;
Tsw=5;
cout<<endl<<" dia: "<<d;
cout<<endl<<" G : "<<G;
cout<<endl<<" rhol: "<<rhol;
cout<<endl<<" rhov: "<<rhov;
cout<<endl<<" mul: "<<mul;
cout<<endl<<" muv: "<<muv;
cout<<endl<<" cpl: "<<cpl;
cout<<endl<<" kl: "<<kl;
cout<<endl<<" sigma: "<<sigma;
cout<<endl<<" hlv: "<<hlv;
cout<<endl<<" Tsw: "<<Tsw;
cout<<endl<<"Do you want to change? [y/n] : ";
if(tolower(getche())=='y')
{
cout<<endl<<"Enter the tube diameter 'd': ";
```

```
cin>>d;
cout<<endl<<"Enter the mass velocity 'G': ";
cin>>G;
cout<<endl<<"Enter the liquid density, rhol: ";
cin>>rhol;
cout<<endl<<"Enter the vapour density, rhov: ";
cin>>rhov;
cout<<endl<<"Enter the liquid viscosity, mul: ";
cin>>mul;
cout<<endl<<"Enter the vapour viscosity, muv: ";
cin>>muv;
cout<<endl<<"Enter liquid specific heat, cpl: ";
cin>>cpl;
cout<<endl<<"Enter the liquid thermal conductivity, 'kl': ";
cin>>kl;
cout<<endl<<"Enter the surface tension, sigma: ";
cin>>sigma;
cout<<endl<<"Enter the latent heat of vaporisation, hlv: ";
cin>>hlv;
cout<<endl<<"Enter the temperature difference, Tsw: ";
cin>>Tsw;
}
prndl = mul*cpl/kl;
wfno = g*d*d*rhol/sigma;
```

```
A = M_PI_4 * d*d;
cout <<endl<< "x" <<'\t'<< "eps" <<'\t'<< "Gwavy" <<'\t' << "xia" <<'\t'<< "Gstr"
<<'\t'<< "Gmist" <<'\t'<< "Gbubly" <<'\t'<< "Pattern" << '\t'<<"htp";
for(x=0.03;x<0.95;x+=0.01)
{
epsh = 1/(1+((1-x)/x)*(rhov/rhol));
epsra = (x/rhov)/((1.+0.12*(1-x))*(x/rhov+(1-x)/rhol)+(1.18*(1-x)*(pow(g*sigma*(rhol-
rhov),0.25 )))/(G*pow(rhol,0.5)));
if (epsh==epsra)
        eps=epsh;
else
        eps=(epsh-epsra)/log(epsh/epsra);
        Ald = A*(1-eps)/d/d;
        Avd = A*eps/d/d;
theta_str = 2*M_PI-2*(M_PI*(1-eps)+pow(3*M_PI/2,(1./3))*(1.-2*(1-eps)+pow(1-
eps,(1/3.))-pow(eps,(1./3)))-(1/200.)*(1-eps)*eps*(1-2*(1-eps))*(1+4*(pow(1-eps,2)+
pow(eps,2))));
hld = (1-cos((2*M_PI-theta_str)/2))/2;
pid = sin((2*M_PI-theta_str)/2);
Gwavy = pow((16*pow(Avd,3)*g*d*rhol*rhov)/(x*x*M_PI*M_PI*pow(1-pow(2*hld-
1,2),0.5))*(M_PI*M_PI/(25*hld*hld)*pow(wfno,-1.023)+1),0.5)+50-75*exp(-pow(x*x-
0.97,2)/(x*(1-x)) );
Gstr=pow((const1*Ald*Avd*Avd*rhov*(rhol-rhov)*mul*g)/(x*x*(1-x)*pow
(M_PI,3)),(1./3))+20*x;
xia = 1/(1+0.2914*pow(rhov/rhol,-1/1.75)*pow(mul/muv,(-1./7)));
```

```
zeta = pow((1.138+2.0*log(M_PI/(1.5*Ald))) ,-2);

Gmist= pow(((7680*Avd*Avd*g*d*rhol*rhov)/(x*x*M_PI*M_PI*zeta))/wfno,0.5

Gbubly = pow((256*Avd*Ald*Ald*pow(d,1.25)*rhol*(rhol-rhov)*g)/(0.3164*pow
x,1.75)*M_PI*M_PI*pid*pow(mul,0.25)),(1/1.75));

out <<endl<< x <<'\t'<< eps <<'\t'<< Gwavy <<'\t' << xia <<'\t'<< Gstr<<'\t'<< G
<<'\t'<< Gbubly <<'\t';

if(G>Gwavy && G<Gmist && x>xia)

{

flow=annular;

out<< "Annular";

}

else if(G>Gwavy && G<Gmist && x<xia)

{

flow=intermittent;

out<< "Intermittent";

}

else if(Gstr<G && G<Gwavy)

{

flow=stratified_wavy;

out<< "Stratified wavy";

}

else if (G<Gstr)

{

flow=stratified;

out<< "Stratified";
```

```
else
{
flow=mist;
out<< "Mist";
}
del = d*(1-eps)/4;
Rel = G*d*(1-x)/mul;
ul = G*(1-x)/(rhol*(1-eps));
uv = G*x/(rhov*eps);
if(flow==stratified)
        fi = 1+pow(uv/ul,(1./2))*pow(((rhol-rhov)*g*del*del/sigma),(1./4))*(G/Gstr);
else
        fi = 1+pow(uv/ul,(1./2))*pow(((rhol-rhov)*g*del*del/sigma),(1./4));
/* heat transfer coefficient for axial flow*/
h_c=0.00324*pow(Rel,0.74)*pow(prndl,0.5)*(kl/del)*fi;
/* heat transfer coefficient for gravitational flow*/
h_f = 0.728*pow(eps,3.0/4)*pow(rhol*(rhol-rhov)*g*hlv*pow(kl,3)/
(mul*d*Tsw),(1./4));
if(flow==annular || flow==intermittent || flow==mist)
 theta = 0;
else if(flow==stratified_wavy)
 theta=theta_str*pow((Gwavy-G)/(Gwavy-Gstr),0.5);
else
```

```
 theta=theta_str;
/*Heat transfer coefficient for two-phase flow*/
htp = ((h_f*(d/2)*theta)+((2*M_PI-theta)*(d/2)*h_c))/(M_PI*d);
out<<'\t'<< htp;
}
return 0;
}
```

```
zeta = pow((1.138+2.0*log(M_PI/(1.5*Ald))) ,-2);

Gmist= pow(((7680*Avd*Avd*g*d*rhol*rhov)/(x*x*M_PI*M_PI*zeta))/wfno,0.5);

Gbubly = pow((256*Avd*Ald*Ald*pow(d,1.25)*rhol*(rhol-rhov)*g)/(0.3164*pow(1-
x,1.75)*M_PI*M_PI*pid*pow(mul,0.25)),(1/1.75));

out <<endl<< x <<'\t'<< eps <<'\t'<< Gwavy <<'\t' << xia <<'\t'<< Gstr<<'\t'<< Gmist
<<'\t'<< Gbubly <<'\t';

if(G>Gwavy && G<Gmist && x>xia)

{

flow=annular;

out<< "Annular";

}

else if(G>Gwavy && G<Gmist && x<xia)

{

flow=intermittent;

out<<  "Intermittent";

}

else if(Gstr<G && G<Gwavy)

{

flow=stratified_wavy;

out<<  "Stratified wavy";

}

else if (G<Gstr)

{

flow=stratified;

out<<  "Stratified";
```

```
}
else
{
flow=mist;
out<<  "Mist";
}
del = d*(1-eps)/4;
Rel = G*d*(1-x)/mul;
ul = G*(1-x)/(rhol*(1-eps));
uv = G*x/(rhov*eps);
if(flow==stratified)
        fi = 1+pow(uv/ul,(1./2))*pow(((rhol-rhov)*g*del*del/sigma),(1./4))*(G/Gstr);
else
        fi = 1+pow(uv/ul,(1./2))*pow(((rhol-rhov)*g*del*del/sigma),(1./4));
/* heat transfer coefficient for axial flow*/
h_c=0.00324*pow(Rel,0.74)*pow(prndl,0.5)*(kl/del)*fi;
/* heat transfer coefficient for gravitational flow*/
h_f = 0.728*pow(eps,3.0/4)*pow(rhol*(rhol-rhov)*g*hlv*pow(kl,3)/
(mul*d*Tsw),(1./4));
if(flow==annular || flow==intermittent || flow==mist)
  theta = 0;
else if(flow==stratified_wavy)
  theta=theta_str*pow((Gwavy-G)/(Gwavy-Gstr),0.5);
else
```

```
 theta=theta_str;
/*Heat transfer coefficient for two-phase flow*/
htp = ((h_f*(d/2)*theta)+((2*M_PI-theta)*(d/2)*h_c))/(M_PI*d);
out<<'\t'<< htp;
}
return 0;
}
```
